RSC Advances

REVIEW

View Article Online
View Journal | View Issue

Cite this: *RSC Adv.*, 2025, **15**, 19762

Recent exploration of inorganic sonosensitizers for sonodynamic therapy of tumors

Conghao Liu,†[ab] Xueyu Liu,†[ab] Ling Zha,†[c] Yulong Zhang,†[ab] Ruizhuo Ouyang,[*ab] Dong Sun*[d] and Yuqing Miao[*ab]

With the rapid development of nanomedicine and nanobiotechnology, various therapeutic methods have been applied with good efficacy and biological safety. As a non-invasive treatment method, sonodynamic therapy (SDT) can effectively treat deep tumors with less damage to the surrounding tissue and high adaptability. The ultrasound sensitizer is an indispensable and important part of the SDT process, and its structure and properties directly determine the therapeutic effect of SDT. Compared with conventional organic sonosensitizers, inorganic sonosensitizers including noble metal-based, transition metal-based, silicon-based and carbon-based sonosensitizers have high stability, controllable morphology and long circulation time in the human body, which has greatly expanded their research applications in SDT. In this review, the possible mechanisms of SDT, *i.e.* the cavitation effect and the generation of reactive oxygen species, are briefly discussed. Subsequently, recent research progress of inorganic sonosensitizers is systematically summarized in terms of their formulations and antitumor effects with a focus on strategies to optimize therapeutic efficacy. The current challenges and future are presented to provide insights into strengthening the interdisciplinary collaborations so as to promote the innovation and development of SDT technology in clinical application.

Received 3rd March 2025
Accepted 17th April 2025

DOI: 10.1039/d5ra01501d

rsc.li/rsc-advances

1 Introduction

Currently, cancer remains one of the most important diseases threatening human life and health.[1] It is known that cancer develops through a multi-step pathological process involving changes in many cellular physiological systems, such as cell differentiation and apoptosis.[2] Cancers initially start as localized diseases, but their tendency to spread to distant parts of the body makes them difficult to cure.[3] Conventional cancer treatments include surgical removal, chemotherapy (CT) and radiotherapy (RT).[4] While all of these treatments have achieved good clinical results, they all cause varying side effects after treatment. For example, surgical resection is the most direct and effective treatment for most solid tumors.[5] However, resection can cause acute pain at the incision site, and the tumor tissue or cells remaining after surgery usually re-develop into solid tumors locally or distantly, leading to tumor recurrence or metastasis;[6] chemotherapy is a form of adjuvant tumor treatment that mainly inhibits further growth and division of cancer cells.[7] Due to the poor solubility and specificity of chemotherapeutic agents, they cannot be targeted directly against cancer cells, which leads to severe toxic effects.

With the development and application of novel nanotechnology platforms, researchers have developed a variety of cancer treatments based on the unique benefits of nanomaterials.[8] For example, researchers have developed various types of nanophotothermal sensitizers for photothermal therapy (PTT) of tumors that can be heated to kill tumor cells under specific light irradiation.[9] Similarly, small molecule photosensitizers for photodynamic therapy (PDT) can induce apoptosis and necrosis of tumor cells when the photosensitizer is activated to generate reactive oxygen species (ROS) under irradiation with light of specific wavelengths.[10] Although PDT reduces the side effects of conventional cancer therapies on the human body to a certain extent, its effectiveness in treating deep-seated tumors is limited due to the low penetration depth of PDT, and its therapeutic spectrum may not include deep-seated tumors.[11]

Sonodynamic therapy (SDT) is a non-invasive treatment method that triggers cell death through the generation of ROS by sonosensitizers under the influence of ultrasound (US). In 1989, Yumita and Umemura[12] discovered that hematoporphyrin (HP) can be activated by US to kill tumor cells. Since then, SDT has been considered the most promising treatment method for tumors.[13] US is often used as a mechanical wave in biomedical fields.[14] With SDT, the ultrasound can penetrate deep into the

[a]*Institute of Bismuth and Rhenium Science, University of Shanghai for Science and Technology, Shanghai 200093, China. E-mail: ouyangrz@usst.edu.cn; yqmiao@usst.edu.cn*

[b]*USST-UH International Joint Laboratory for Tumor Diagnosis and Energy Treatment, University of Shanghai for Science and Technology, Shanghai 200093, China*

[c]*Department of Laboratory Diagnosis, Changhai Hospital, Naval Medical University, Shanghai 20043, P. R. China*

[d]*Henan Normal University, Xinxiang 453007, China. E-mail: sundong2004@126.com*

† C. Liu, X. Liu, L. Zha and Y. Zhang contributed equally to this work.

tissue and focus precisely on the tumor cells, which in turn stimulates the acoustic sensitizer to generate ROS that kill the tumor cells. SDT offers two key advantages: (1) deeper tissue penetration with spatial precision, and (2) minimized damage to surrounding healthy tissues.[15]

In the course of the development of nanotechnology, sonosensitizers are frequently used to control SDT[15] due to their strong imaging capability. Sonosensitizers play a crucial role in the process of SDT. sonosensitizers can be enriched and generate cytotoxic ROS in the tumor region under the influence of US, which in turn triggers apoptosis and necrosis of tumor cells and achieves the killing effect on tumor cells.[16] The currently known sonosensitizers are mainly organic sonosensitizers and inorganic sonosensitizers.[17] Initially, photosensitizers such as Hp, hematoporphyrin monomethyl ether,[18] Gaporphyrin,[19] photoporphyrin IX,[20] and other porphyrin derivatives used in PDT were used directly as sonosensitizers for SDT.[21] Subsequently, xanthones,[22] organic compounds with specific chemical structures, have also shown some acoustic sensitization. In addition, several antitumor drugs, including doxorubicin (DOX),[23] curcumin,[24] and artemisinin,[25] have been investigated as sonosensitizers for SDT to enhance the killing effect on tumor cells after US activation.[26]

Organic sonosensitizers have only a limited therapeutic effect of SDT due to their hydrophobicity, non-specificity, and short residence time in the body, which leads to insufficient accumulation at the tumor site. In contrast to organic sonosensitizers, recently developed inorganic sonosensitizers, such as titanium dioxide (TiO_2) nanoparticles,[27] manganese dioxide (MnO_2) nanoparticles,[28] and ultrasmall quantum dots (QDs), have been well developed in terms of improved chemical stability, and phototoxicity, and offer a broad perspective for the application of SDT. as shown below. (1) Due to their unique semiconducting properties, inorganic sonosensitizers are able to trigger the production of electrons (e^-), and holes (h^+) under certain conditions, leading to the generation of ROS.[29] (2) Inorganic sonosensitizers exhibit excellent stability in physiological environments, and can circulate in the body for long periods without being rapidly degraded.[30] (3) They are relatively easy to control in terms of size, and morphology, which facilitates further biomedical applications such as tumor targeting or drug delivery.[31] Despite the above advantages of inorganic sonosensitizers, the SDT efficiency of most modern inorganic sonosensitizers is still unsatisfactory. To improve the SDT efficiency of inorganic sonosensitizers, the development of suitable sonosensitizers has become an important topic of current research.

Here we provide an overview of the latest developments in inorganic sonosensitizers. First, the potential therapeutic mechanisms of sonodynamic therapy are discussed in detail. Then, the current design, synthesis, and biological effects of inorganic sonosensitizers (based on noble metals, transition metals, carbon (C), and silicon (Si) (Fig. 1)) are discussed and some constructive ideas to improve their therapeutic efficiency for SDT are presented. Finally, challenges and key issues in this field for the future development of SDT are discussed.

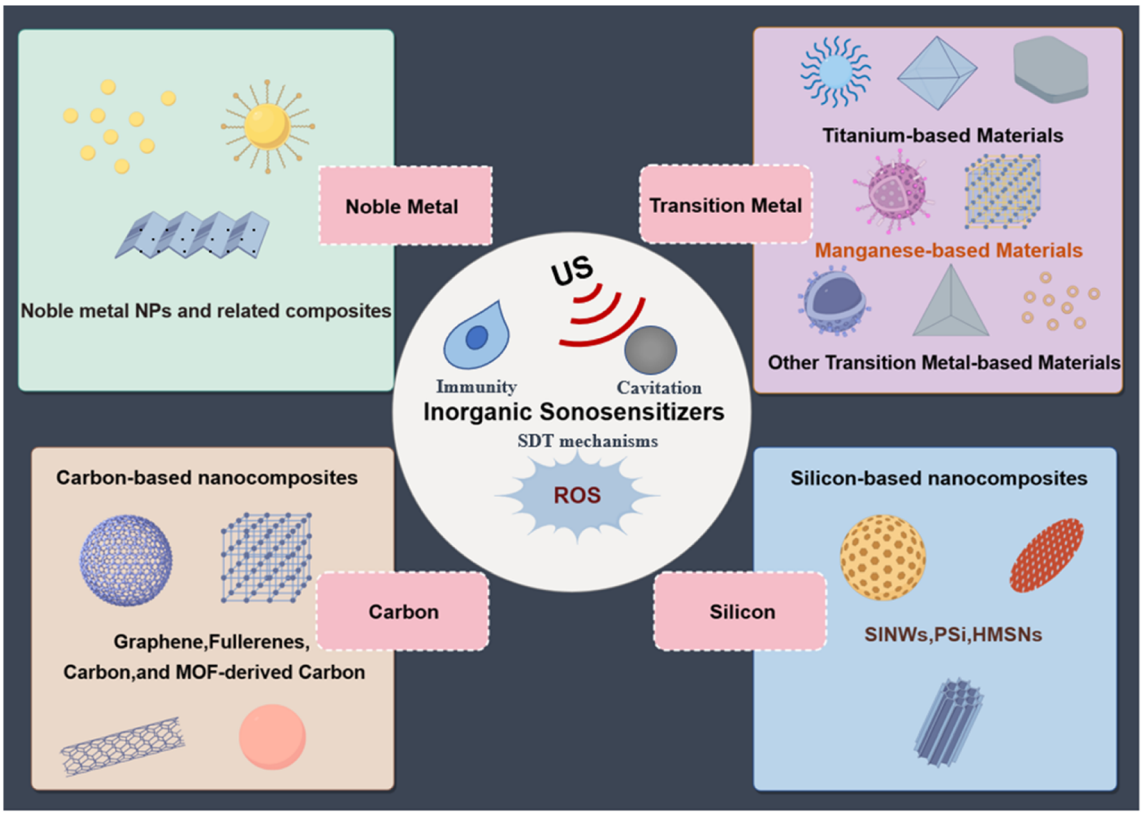

Fig. 1 Mechanism of sonodynamic therapy.

2 Mechanisms of acoustic energy therapy

The mechanism of SDT has been much discussed in recent years, but due to the complexity of the process, its exact mode of operation remains unclear. (1) US-induced cavitation effect, and (2) ROS generation is the possible mechanisms of SDT. The most widely accepted mechanism is the generation of ROS induced by pyrolysis or acoustic luminescence (Fig. 2).

2.1 Cavitation effects

The cavitation effect, also known as ultrasonic cavitation, refers to the vibration of microscopic gaseous cavitation bubbles (also known as cavitation nuclei) in a liquid in the presence of sound waves. When the sound pressure reaches a certain level, these cavitation bubbles undergo a kinetic process of growth and decay. During this process, the cavitation bubbles undergo a series of changes such as oscillation, expansion, contraction, and bursting[32] releasing enormous energy. There are two types of cavitation effects: inertial cavitation and stable cavitation.[33] In inertial cavitation, the cavitation bubbles expand and contract rapidly under the action of high-intensity ultrasonic waves, which eventually leads to the bursting of the bubbles. During this process, enormous amounts of energy are released, generating shock waves, acoustic luminescence, and localized high-temperature and high-pressure environments. These extreme conditions can activate sonosensitizers and promote the production of ROS,[34] ultimately leading to the lysis of cancer cells. In contrast, stable cavitation is a process in which the cavitation bubbles are continuously vibrated in a small area by low-intensity ultrasound, and this vibration increases the rate of diffusion of the nuclear gases, facilitating the translocation of charge carriers into the cell. Stabilized cavitation is primarily used in SDT in combination with sonosensitizers to achieve therapeutic effects targeting the focal point, including targeted release of carrier drugs and enhancement of drug uptake, penetration, and alteration of the immune microenvironment.[35] The cavitation effect has a broad application perspective in sound power therapy. On the one hand, tumor cells can be killed directly and indirectly to improve the therapeutic effect; on the other hand, the permeability of cell membranes can be altered and the targeting accuracy and permeability of sonosensitizers[15] can be improved. With the continuous development of molecular imaging and molecular biology, as well as the constant advances in ultrasound technology and nanotechnology, the application of the cavitation effect in sound therapy will become more extensive and profound. Ultrasonic microbubbles as optimal cavitation nuclei can significantly enhance and precisely regulate the cavitation effect. In the future, the application of the cavitation effect in sound power therapy will become even more promising with the continuous progress of the corresponding technologies.

2.2 ROS generation

Sonosensitizers are stimulated by the US to transfer energy to molecular oxygen (O_2), which in turn generates different types of ROS, *e.g.* singlet oxygen ($^1O_2$), superoxide anions (O_2^-), and

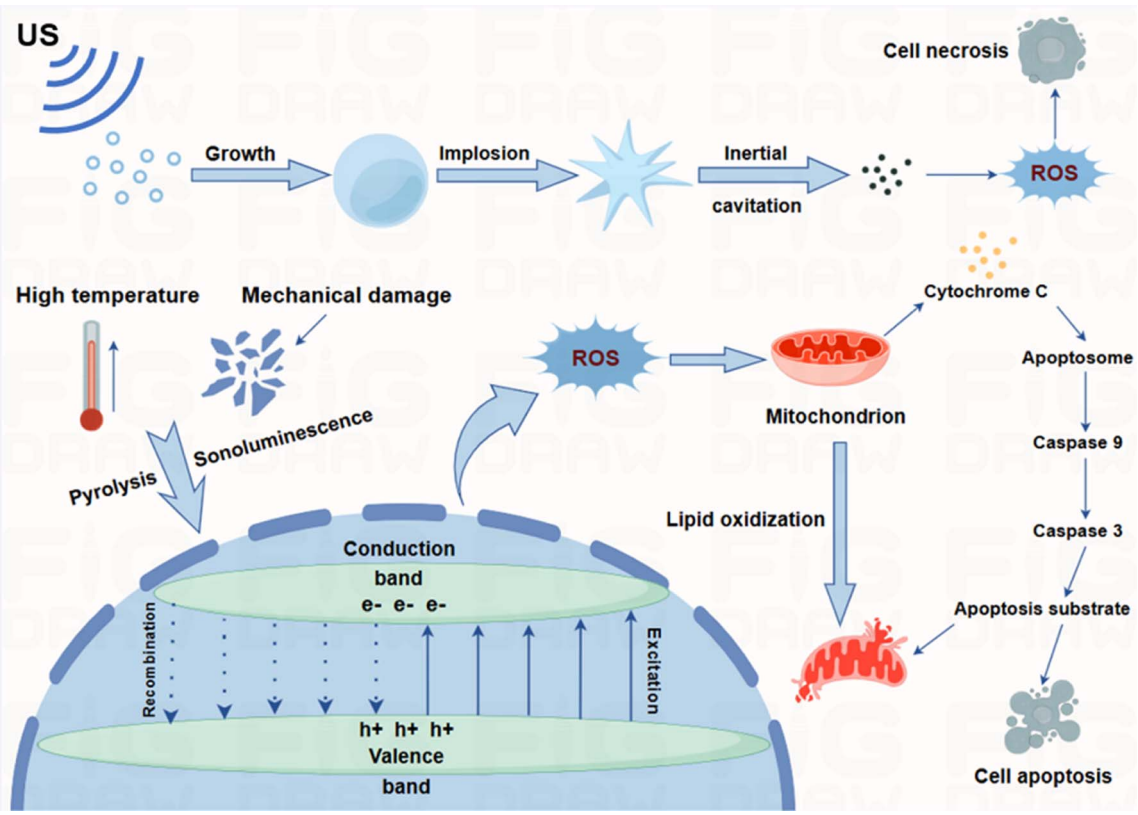

Fig. 2 Schematic illustration of possible mechanisms of SDT.

hydroxyl radicals (·OH).[36] These reactive oxygen species can cause cell damage and trigger apoptosis in cancer cells. ROS production[37] is one of the most important steps in SDT. Currently, cavitation is considered the main process of reactive oxygen species production by sonosensitizers under US exposure. The most widely accepted mechanism is pyrolysis or acoustic luminescence-induced ROS production.[38] Specifically, pyrolysis occurs when microbubbles burst during the cavitation effect, releasing large amounts of energy and interacting with the surrounding liquid; this interaction leads to pyrolysis of the liquid, resulting in the formation of ROS.[35] Acoustic luminescence occurs in the inertial cavitation process, the sharp collapse of the bubble will produce acoustic luminescence phenomenon. Acoustic luminescence is a phenomenon in which light radiation is excited by ultrasound, causing the acoustic sensitizer to transition from the ground state to an excited state. When the activated acoustic sensitizer returns to the ground state, it releases energy that is transferred to the surrounding oxygen, resulting in the formation of large amounts of reactive oxygen species.[39] In both mechanisms, the high temperature and pressure generated when the bubbles burst lead to sonochemical effects that generate ROS and damage mitochondrial membranes by promoting lipid peroxidation, resulting in a decrease in mitochondrial membrane potential and an increase in membrane permeability.[37] In addition, cytochrome c released from the damaged mitochondrial membrane activates the apoptotic signaling pathway, which ultimately leads to the apoptosis of cancer cells. Although experimental evidence supports both pathways of ROS generation, it is not clear which pathway is the main mechanism of ROS generation in SDT. This remains an important area of research, and further experimental and theoretical studies are needed to uncover the exact mechanism of ROS generation in SDT. A more comprehensive understanding of ROS generation pathways will help to develop and apply sonosensitizers more effectively, thereby improving the therapeutic efficacy and safety of SDT. In summary, ROS generation in SDT is a complex and interesting process involving multiple physical and chemical mechanisms. Future studies will focus on uncovering the intrinsic relationships and interactions between these mechanisms, providing a more solid theoretical basis for the clinical application of SDT.

Notably, the tumor microenvironment (TME) critically modulates SDT efficacy. Hypoxia, a hallmark of solid tumors, may limit O_2 availability for ROS generation, particularly for sonosensitizers relying on type II photodynamic pathways. Recent studies suggest that MnO_2-based sonosensitizers can alleviate hypoxia by catalyzing H_2O_2 decomposition to O_2.[40] Additionally, the acidic TME (pH 6.5–7.0) could influence charge states of transition metal-based sonosensitizers, altering their catalytic activity. Redox homeostasis, maintained by elevated glutathione (GSH) levels in tumors, also necessitates sonosensitizers with GSH-depleting capabilities.

3 Inorganic nanomaterials in sound power therapy

SDT is a new non-invasive tumor treatment in which US is used to stimulate the acoustic sensitizer to generate ROS that induce tumor cell death to achieve the therapeutic goal. Sonosensitizers play a crucial role in SDT. In recent years, inorganic nanostructures such as noble metals, transition metal oxides, carbon-based and silicon-based materials have been used as sonosensitizers with remarkable results due to their high stability and special physicochemical properties. The recent advances in these inorganic sonosensitizers are reviewed below in terms of design principles to improve their therapeutic efficacy:

3.1 Noble metal-based sonosensitizers

The unique physicochemical properties of metal-based sonosensitizers as a key component in SDT, in particular their high stability, good electron transfer capability and catalytic activity, enable these materials to efficiently generate ROS under ultrasound irradiation, which in turn induce apoptosis or necrosis of tumor cells. Metal-based sonosensitizers usually have high stability and special physicochemical properties, such as good electron transfer capability and catalytic activity, which make them potentially useful for SDT. Various noble metal nanoparticles such as gold, silver, and platinum nanoparticles and their modified forms are considered excellent sonosensitizers due to their high stability, good water solubility, non-dermal photosensitization and inherent acoustic cavitation properties.

3.1.1 Au-based materials. Among the various novel metallic nanoparticles, gold nanoparticles exhibit a unique set of favorable properties for SDT, including tunable optical and thermal properties, low toxicity, good cellular uptake, excellent biocompatibility and anti-angiogenic properties. These properties make gold nanoparticles attractive candidates for SDT and should provide new ideas and strategies for tumor therapy. In 2013, the first use of AuNPs for SDT was proposed and investigated by Sazgarnia[41] *et al.* They found[42] that AuNPs enhance acoustic cavitation in the presence of intense pulsed light, which could significantly reduce the relative tumor volume and thus improve therapeutic efficacy in colorectal cancer. This is due to the special optical properties of AuNPs, which can generate vapor bubbles in the presence of intense pulsed light, forming core sites for acoustic cavitation and effectively enhancing the effect of tumor treatment. However, the experimental results showed that the therapeutic effect on the tumor in the group with Au-NP and US was not particularly pronounced and that additional intense irradiation with pulsed light was required to promote vapor bubble formation and achieve a US response. Therefore, pure AuNPs can only achieve limited therapeutic effects in SDT and often need to be further modified or synergized with other therapeutic modalities to effectively enhance SDT. Loke *et al.*[43] reported for the first time that AuNRs encapsulated in alginate (Au NRs^{ALG}) have improved biocompatibility and can be effectively used as a nanoacoustic sensitizer for SDT. The ultrasound-activatable $AuNRs^{ALG}$ catalyzed ROS production *via* the mitochondrial cell death pathway and caused severe DNA damage to cancer cells, triggering apoptosis (Fig. 3a). Under US irradiation (1.0 W cm^{-2}, 5 min), the Au NRs^{ALG} structure remained stable and structurally intact for three cycles. The experimental results showed that US irradiation (1.0 W cm^{-2}, 5 min) could

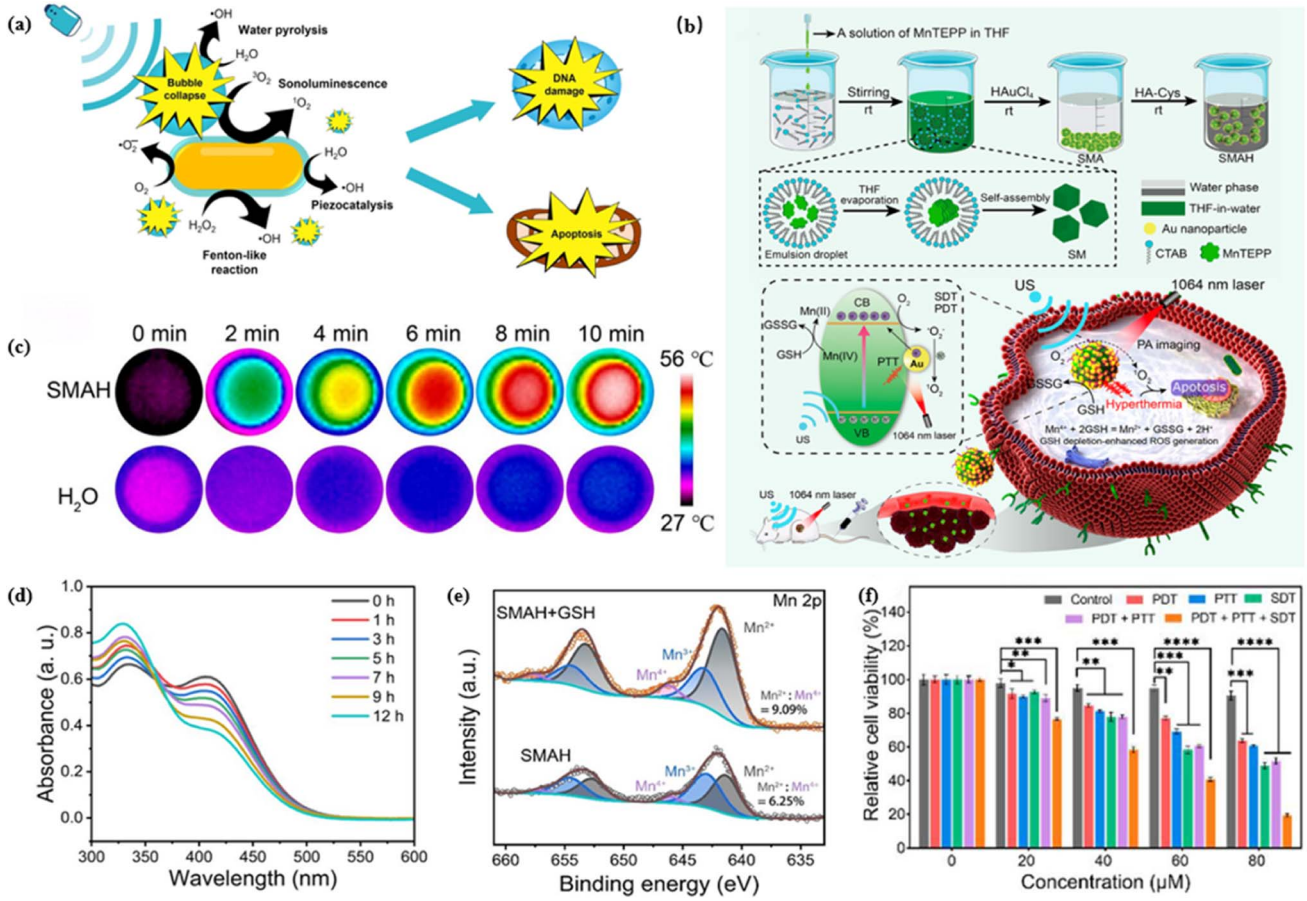

Fig. 3 (a) Schematic representation of the acoustic catalytic effect of Au NRs^{ALG} on cancer cells. Ultrasound-activatable Au NRs^{ALG} catalyzes the production of ROS through the mitochondrial cell death pathway, leading to severe DNA damage and triggering apoptosis in cancer cells; Copyright 2023, Elsevier.[43] (b) Schematic illustration of the synthesis process of self-assembled SM nanoparticles and SMAH heterostructures; shows the mechanism of photocatalytic, acoustic catalytic and anti-tumor effects of SMAH heterostructures; (c) infrared thermal images of SMAH (80 μM) aqueous solution and water using 1064 nm light irradiation; (d) consumption of GSH by SMAH with DTNB as scavenger at different reaction times; (e) XPS spectra of Mn 2p peaks in SMAH before and after incubation with GSH; (f) cell viability of 4T1 cells after different treatments. Copyright 2024, American Chemical Society.[40]

significantly enhance the cavitation effect, and the generated $^1O_2$ was 3–8 times higher than that of other commercially available titanium dioxide nanosonosensitizers[44] AuNRs^{ALG}-mediated SDT proved to be a promising therapeutic approach due to its good biocompatibility, non-invasiveness and deep tissue penetration, in addition to its well-established role as a photosensitizer and photothermal sensitizer. The above-mentioned AuNPs-based sonosensitizers aggregate in the tumor region through increased permeability and retention effects, but accumulation at deeper tumor sites is usually limited, which may result in lower therapeutic efficacy. In recent years, tumor treatment is often performed by combining SDT with PTT,[45] which can take advantage of the synergistic effects of the two to further improve the efficacy of tumor treatment. Xu *et al.*[40] synthesized manganese porphyrin (SM) nanoparticles with well-defined self-assembled metalloporphyrin networks, and this self-assembled structure enables SM to perform energy transfer and charge separation in catalytic reactions more efficiently.[46] It enables efficient energy transfer for improved photocatalytic and acoustic catalytic activities in $^1O_2$ production. Subsequently, AuNPs were grown *in situ* on the SM surface by anchoring the porphyrin-terminal alkyne group to form a plasma SMA heterostructure, which exhibited excellent absorption and photothermal properties in the near-infrared region (Fig. 3b), and the temperature of the aqueous solution of SMAH reached 56 °C at a concentration of 80 μM, corresponding to an increase of 29 °C, which could promote the separation and transfer of electron–hole pairs and effectively ablate the cancer cells[40] (Fig. 3c). By modifying hyaluronic acid (HA), the heterostructured SMAH nanocomposites have good water solubility and can actively target cancer cells. In addition, the SMAH heterostructures can consume endogenous GSH. The GSH-consuming ability of SMAH was evaluated using the 5,5-dichroic acid (2-nitrobenzoic acid) (DTNB) probe,[47] and the results showed a gradual decrease in characteristic absorbance at 412 nm with the gradual increase in incubation time (Fig. 3d), indicating that SMAH can effectively consume GSH. The XPS spectra of SMAH before and after incubation with GSH were further determined, and the state ratio of Mn^{2+} to Mn^{4+} increased from 6.25% to 9.09% in GSH-activated SMAH

(Fig. 3e), indicating that the decreased power of GSH[48] disturbed the redox balance and decreased the antioxidant capacity of tumors and further increased the $^1O_2$ production rate during SDT and PDT. Under the irradiation of NIR-II light and US, SMAH produced thermotherapy and a large amount of $^1O_2$, resulting in cancer cell damage. Experimental results showed that the lowest survival rate of 4T1 cells treated with 80 μM SMAH + 1064 nm laser + US was 17.83% (Fig. 3f), and both *in vitro* and *in vivo* studies confirmed that the SMAH nanocomposites effectively inhibited tumor growth by decreasing GSH levels in SDT-enhanced PDT/PTT. This work provides a paradigm for increasing the $^1O_2$ yield of metalloporphyrin to enhance the synergistic therapeutic effect of SDT/PTT/PDT, effectively increasing the therapeutic effect on the tumor.

3.1.2 Ag-based materials. Silver nanoparticles (Ag NPs) are the most discussed nanomaterials in nanomedicine.[49] Ag NPs are frequently used in antimicrobial therapy studies as they have significant bactericidal properties against Gram-negative, Gram-positive and anaerobic bacteria.[50] At the same time, Ag NPs also have antitumor capabilities by inducing the production of ROS to regulate oxidative stress, as well as impairing energy metabolism and multidrug resistance, ultimately leading to cell death. In previous studies, Ag NPs were often activated by laser irradiation to generate ROS and thus enable photodynamic therapy of tumors.[51] For example, Mysara *et al.*[52] reported on Ag-modified S-doped g-C_3N_4 composites with enhanced photocatalytic activity under solar irradiation, which exhibit high ROS generation efficiency. However, photodynamic therapy is not suitable for the treatment of deep tumors. Therefore, researchers have started to explore the application of Ag NPs in SDT, which uses ultrasound as an activation source and is more suitable for deep tumor[53] therapy than PDT due to its ability to penetrate deeper into the tissue. For example, Liang *et al.*[54] found that the combination of US + Ag NPs (<100 nm) significantly reduced the viability of human ovarian cancer cells compared to Ag NPs or US alone. Meng *et al.*[55] found that a metal–organic backbone (MOF), which can effectively act as a negative carrier for sonosensitizers and rapidly disseminate ROS, has great potential for SDT. They reported the design of MIL@Ag heterostructures, *i.e.*, *in situ* modification of Ag NPs on the surface of MIL (MOF(Ti)), strategically fabricated MIL@Ag heterostructures as acoustic nanosensitizers, and Ti-based MOFs with high porosity and high surface area by hydrothermal synthesis using H_2BDC-NH_2 as the organic ligand and Ti(Oi-Pr)$_4$ as the metal compound (MIL). The high content of amino groups in the MOFs favors the *in situ* growth of Ag NPs to build MIL@Ag heterostructures[56] (Fig. 4a). When MIL@Ag was exposed to US irradiation, MIL@Ag exhibited more efficient charge transfer and lower O_2 adsorption capacity compared to bare MIL, while the charge of Ti metal nodes in MIL could be transferred to the Ag NPs, which attenuated the recombination of electron–hole pairs and generated more efficient charge reactions, enhancing the ability to generate ROS (Fig. 4b). Under US irradiation, the activated electrons of MIL@Ag can reduce the surrounding O_2 and generate $\cdot O_2^-$, while the activated holes can oxidize H_2O and generate $\cdot$OH. The therapeutic efficiency of SDT was effectively improved (Fig. 4c). Under US irradiation, MIL@Ag-PEG killed the central cells in MCTS and penetrated the 2 cm thick tissue barrier to kill A549 cancer cells (Fig. 4d). As the thickness of the sarcomere increased, even at a barrier thickness of 2 cm, US irradiation was able to cause extensive damage to cancer cells cultured with MIL@Ag-PEG and produce a distinct red fluorescence associated with apoptotic cells (Fig. 4e). In addition, MIL@Ag-PEG killed pathogenic bacteria at the site of wound infection and promoted wound healing. Thus, MIL@Ag-PEG offers a promising strategy to improve the performance of SDT through rational heterogeneous structure design.

3.1.3 Pt-based materials. Platinum (Pt) NPs have been widely used in anti-tumor sonic therapy studies. By injecting sonosensitizers containing Pt NPs and applying ultrasound, ROS can be generated to kill tumor cells.[57] Currently, the combination of noble metal nanoparticles with metal–organic complexes[57,58] to explore new properties in biomedical applications is receiving much attention. Sun *et al.*[59] investigated and developed a simple coordination crystallization method to prepare Pt-anchored metal–organic complexes (Pt-MOCs) nanoparticles (Fig. 5a). By directly mixing disulfide ether (DSF), chloroplatinate and a reducing agent. Pt-MOCs By incorporating Pt NPs on the surface of MOCs, the quantum yield of generating $^1O_2$ in the linear state under US was effectively increased, which effectively promoted the apoptosis of cancer cells (Fig. 5b). *In vitro* experiments showed that Pt-MOCs effectively generate $^1O_2$ under the US irradiation and are more cytotoxic to tumor cells than metal–organic complexes (MOCs) or platinum nitrogen oxides. The *in vitro* SDT effect of Pt-MOCs was also investigated in the experiments. The experimental results showed that no significant cell damage was observed in either the control or the US group. On the contrary, the cell survival rate in the group (Pt-MOCs + US) decreased to 28.8%, indicating that Pt-MOCs play an important role in inhibiting the proliferation of cancer cells (Fig. 5c). This study provides a convenient strategy for the fabrication of noble metal-loaded metal–organic complex nanospheres with good acoustic-dynamic therapeutic effects on tumors. In recent years, SDT has been widely used to kill tumors by combining synergistic treatments with other therapeutic approaches.[60,61] An *et al.*[62] designed a smart biodegradable nanoplatform for drug delivery with mitochondrial targeting ability, pH-dependent drug release, and enzyme-like catalytic function. They fabricated a biodegradable hollow polydopamine nanoparticle (CDP@HP-T) embedded with Pt NPs[63,64] after being loaded with DOX and Chlore6 (Ce6) and modified with the mitochondria-targeted molecule triphenylphosphine (TPP) (Fig. 5d). This efficient ROS generation platform uses deep penetrating US radiation for irradiation, combined with tumor chemotherapy and SDT for synergistic tumor treatment. The nanoprobe (CDP@HP-T) has many unique advantages as a novel smart ROS-enhanced nanocomposite. The probe has good biocompatibility[65,66] and is able to effectively alleviate tumor hypoxia, which in turn greatly enhances the tumor elimination effect of chemotherapy combined with SDT and represents a new breakthrough in the field of tumor therapy (Fig. 5e). This study provides new ideas for improving conventional ROS treatment in the future.

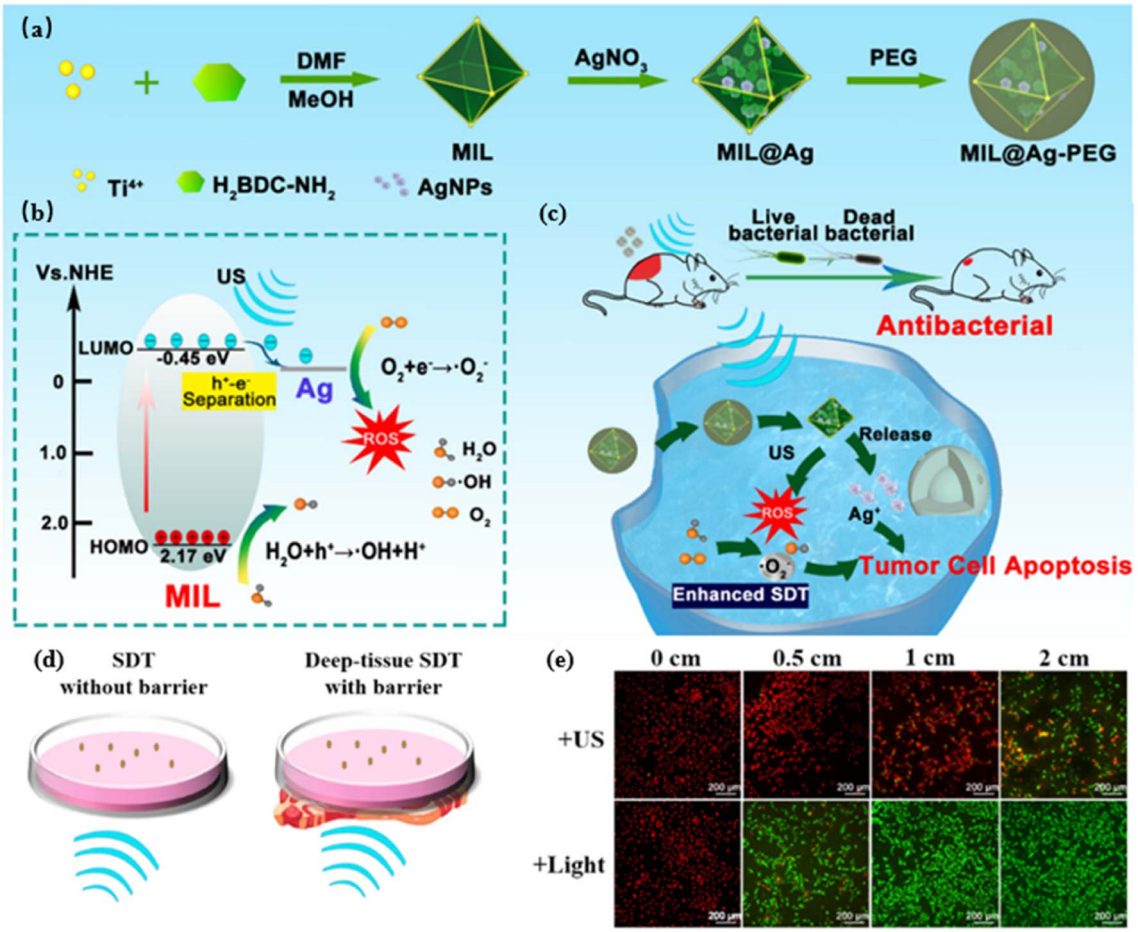

Fig. 4 (a) Schematic preparation process of MIL@Ag-PEG; (b) schematic mechanism of MIL@Ag-PEG for enhancing the mechanism of action of SDT schematic of the mechanism of action of SDT; (c) schematic of the mechanism of MIL@Ag-PEG enhancing the mechanism of SDT for cancer treatment and rapid wound healing; (d) schematic of the MIL@Ag-PEG used to kill the deep cancer cells. Lean meat was used to simulate the barrier to show the SDT and deep tissue SDT settings *in vitro*; (e) CLSM images of A549 cells irradiated with US (2.0 W cm^{-2}) or 635 nm laser light exposed to MIL@Ag-PEG at different thicknesses of the tissue barrier. Copyright 2023, American Chemical Society.[55]

The use of precious metal nanoparticles in SDT has seen advancements in research, but their high cost and limited effectiveness in eliminating tumors have hindered their wide use. However, combining precious metal nanoparticles with other materials, such as PTT or CDT, has proven to be an effective strategy for enhancing the therapeutic efficiency of SDT under ultrasound irradiation. This combination leads to a synergistic effect that significantly improves the anti-tumor efficacy of SDT. The text discusses the impact of combining noble metal nanoparticles with other materials in influencing the properties of the tumor microenvironment, such as pH and redox state. This combination can facilitate the formation and accumulation of ROS, which can be beneficial in cancer treatment. Additionally, when combined with tumor microenvironment-responsive materials, noble metal nanoparticles can more easily penetrate tumor tissue, enhancing the therapeutic effect. However, the high cost and limited availability of noble metal nanoparticles limit their widespread use. As a result, researchers are now focusing on developing high-performance sonosensitizers using non-precious metals as a solution to this challenge.

3.2 Transition metal-based sonosensitizers

Sonosensitizers based on transition metals have great potential for SDT due to their unique electronic structure and chemical properties. They usually have good biocompatibility and stability can be stabilized in living organisms and have therapeutic effects. In addition, due to their energy band structure, transition metal-based sonosensitizers can be easily activated by ultrasound to generate large amounts of ROS, which can have a killing effect on tumor cells. Sonosensitizers based on transition metals have a wide range of applications in the medical field. They can be used not only for the treatment of bacterial infections and viral diseases, but also for the treatment and diagnosis of tumors.[67] By adapting the structure and properties of the sonosensitizers, the generation and release of ROS can be precisely controlled, thereby improving the therapeutic effect and reducing side effects.

3.2.1 Titanium-based materials. Titanium-based materials with good biocompatibility, corrosion resistance, and mechanical properties have significant advantages and are widely used in the biomedical field.[27,68] In recent years,

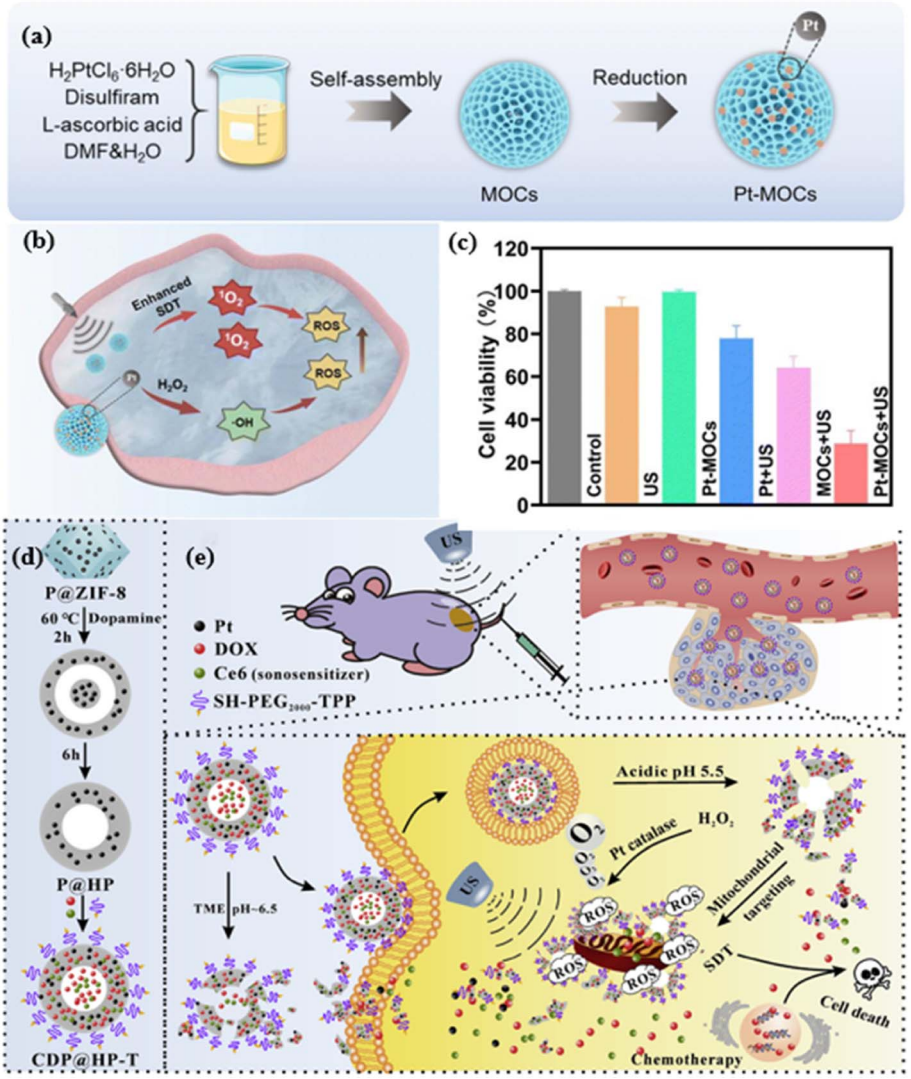

Fig. 5 (a) Schematic representation of Pt-MOCs prepared by coordination crystallization; (b) schematic representation of Pt-MOCs with acoustic sensitization by SDT; (c) cell viability of 4T1 cells incubated with Pt-MOCs under different treatments; Copyright 2023, The Royal Society of Chemistry.[59] (d) Schematic synthesis pathways of CDP@HP-T; and (e) combination of chemotherapy and SDT for CDP@HP-T. Copyright 2020, Elsevier.[62]

titanium-based nanomaterials, especially TiO_2 NPs, have been widely used as highly efficient sonosensitizers for SDT due to their unique physicochemical properties. TiO_2NPs have controllable structures and compositions, improved chemical stability, and are capable of generating ROS[69] under ultrasound (US) irradiation. These ROS mainly include O_2^-, ·OH, and $^1O_2$. Compared to other sensitizers, TiO_2 NPs show excellent results. In 2011, Harada *et al.*[70] from the University of Fukuoka, Japan, reported for the first time that irradiation of melanoma cells with the US in the presence of TiO_2 nanomaterials led to a significant reduction in the viability of melanoma cells. To further optimize this therapeutic effect, they used a polyethylene glycol grafting material containing polyallylamine to modify TiO_2, resulting in the fabrication of a novel core–shell nanomicrobe.[71] This nanocolloid consists of TiO_2 as the core and polyethylene glycol as the shell. The nanocolloid not only improves the dispersion stability of TiO_2 nanoparticles under physiological conditions, but also promotes the uptake of TiO_2 nanoparticles by cervical cancer cells and enhances their killing effect on cervical cancer cells under US irradiation. TiO_2 nanoparticles have low cytotoxicity and excellent chemical stability, making them a promising sensitizer for acoustic sensitization by SDT. However, the ROS quantum yield of untreated TiO_2NPs is not high due to the fast recombination of electrons (e^-) and holes (h^+), which hinders its wide application in SDT. Therefore, the quantum yield of ROS can be improved by facilitating the separation of electron–hole pairs,[72] *e.g.*, by creating oxygen vacancies, connecting noble metals, *e.g.*, Tang *et al.*[73] designed a tumor microenvironment-responsive $CaCO_3$@ Pt–TiO_2 nanocomposite (CaPT) in which they combined Pt NPs and $CaCO_3$ nanoparticles[74,75] to enhance oxidative stress in cancer cells for acoustic kinetic cancer immunotherapy. Pt–TiO_2 NPs[76] were

synthesized *in situ* by growing Pt NPs on the surface of TiO_2 NPs. A $CaCO_3$ layer was then encapsulated on the Pt–TiO_2 NPs to form a CaPT core–shell (Fig. 6a). The Pt NPs could significantly improve the efficiency of TiO_2-mediated ROS generation[77] by preventing electron–hole recombination and also catalyzing the decomposition of H_2O_2 into TME to generate O_2, thereby overcoming tumor hypoxia and enhancing the effect of SDT. The experimental results showed that the TiO_2 NPs had a band gap of 3.2 eV, while the Pt–TiO_2 NPs had a band gap of 3.02 eV. The narrow band gap helps to promote the separation of US-triggered electron (e^-) and hole (h^+) pairs and increase the efficiency of ROS production[78] (Fig. 6b). $CaCO_3$@Pt–TiO_2 (CaPT) nanocomposites respond to the tumor microenvironment and release large amounts of Ca^{2+}, which then enhance oxidative stress and trigger robust activation of tumor immunogenic cell death (ICD)[79] (Fig. 6c). Therefore, SDT-triggered ROS and Ca^{2+} overload could effectively induce ICD and significantly improve the therapeutic effect. In the experimental *in vitro* study, the cell viability of 4T1 cells was measured in groups. The experimental results showed that the cell viability of CaPT + US group (15.3%) was lower than that of Pt–TiO_2 + US group (50.2%) and TiO_2 + US group (65.8%), indicating that Ca^{2+} overload effectively enhanced the antitumor effect of SDT alone (Fig. 6d). In an experimental *in vivo* study in mice, the changes in tumor volume were determined by measuring the changes in tumor volume in mice under different treatment conditions. The results of the study showed that the tumor volume was significantly reduced in the CaPT + US treatment group compared to the other groups (Fig. 6e). CaPT + US treatment showed the most significant tumor elimination at day 14, which was attributed to SDT and Ca^{2+} overload. Both *in vitro* and *in vivo* experiments showed that $CaCO_3$@Pt–TiO_2 nanocomposites can effectively inhibit tumor growth and promote the infiltration of tumor-specific cytotoxic T cells into immunogenic cold tumors.

The combination of SDT and PTT is commonly used for tumor treatment. PTT can generate ROS, while SDT can overcome the limited penetration depth of PTT and target deeper tissue. SDT–PTT combination therapy has shown promise in improving tumor oxygenation, increasing ROS production, and enhancing the thermal sensitivity of cancer cells, resulting in effective tumor treatment. Titanium-based nanomaterials, specifically titanium nitride (TiN) nanodots,[80] have been widely used as sonosensitizers for SDT due to their unique nanostructures and multiple valence states. TiN nanoparticles have demonstrated excellent physicochemical properties, such as good biocompatibility and photothermal characteristics. It is

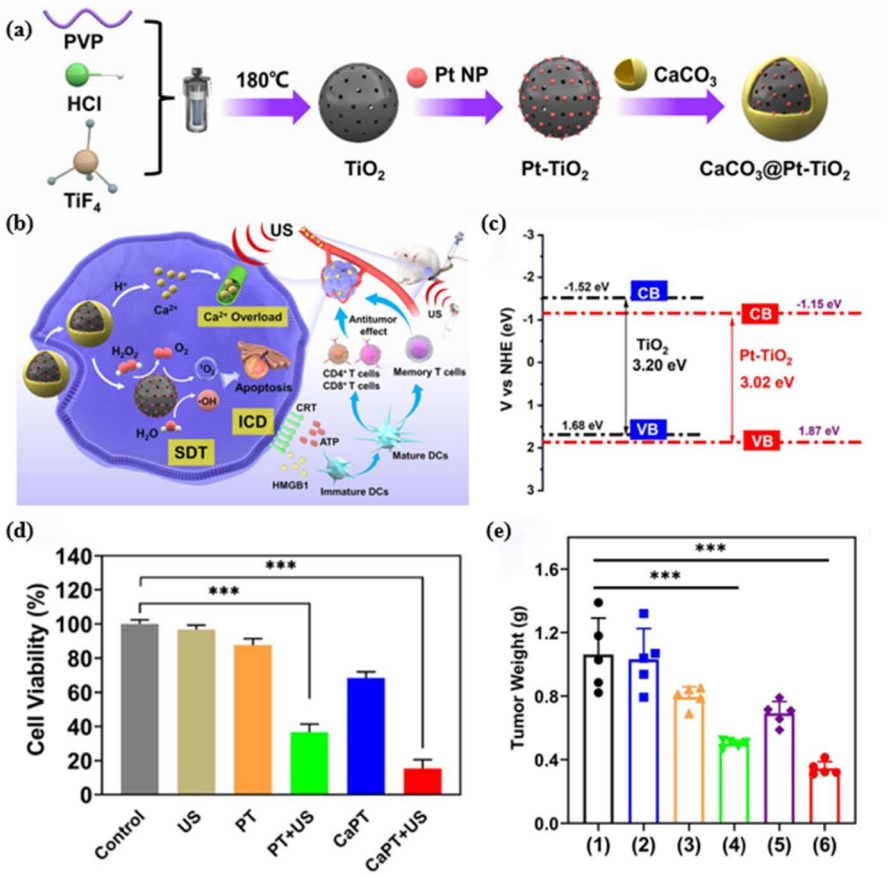

Fig. 6 (a) The synthetic process of $CaCO_3$@Pt–TiO_2 NP; (b) schematic illustration of $CaCO_3$@Pt–TiO_2 NPs for sonodynamic-cooperated immunotherapy; (c) band structures of TiO_2 NPs and Pt–TiO_2 NPs; (d) cell viability of 4T1 cells incubation for 24 h after different treatments; (e) mean tumor volume ((1) control, (2) US, (3) Pt–TiO_2 (PT), (4) PT + US, (5) CaPT, (6) CaPT + US) in each group of loaded nude mice after 14 days of treatment ($n = 5$). Copyright 2023, Elsevier.[73]

worth noting that TiN nanoparticles have vacancies in their crystal lattice structure. In conclusion, the combination of SDT and PTT, using TiN nanodots as sonosensitizers, holds promise for effective tumor treatment due to its ability to enhance ROS production and penetrate deeper tissues. The electron cloud is unevenly distributed around the vacancies, resulting in a lack of electric dipoles, which enhances microwave-excited thermoacoustic therapy. Wang *et al.*[81] successfully synthesized ultra-small TiN nanodots[82,83] for PTT-enhanced synergistic SDT against cancer.[84] First, they synthesized ultra-small TiN nanodots with an average size of 1.5 nm using the liquid stripping method[85] (Fig. 7a). The fabricated TiN nanodots have secondary heat-absorbing properties in the near-infrared region and are oxidized to TiO_2 (ref. 86) due to their special low-oxygen structure and surface fraction. Therefore, the TiN nanodots can be used not only for photoacoustic imaging and photothermal therapy of tumors, but also as efficient sonosensitizers to enhance the separation of e^- and h^+ from the energy band structure under US irradiation, leading to the good SDT performance of TiN nanodots (Fig. 7b). TiN nanorods induce mild photothermal heating of the tumor under near-infrared laser irradiation, which in turn promotes tumor blood flow and improves tumor oxygenation, leading to a stronger effect of the combined PTT and SDT treatment. The ultra-small size of TiN nanodots, most of which can be rapidly degraded in mice, also reduces concerns about the long-term toxicity of nanomaterials (Fig. 7d). They first designed a treatment protocol for PTT–SDT with TiN nanodots in a 4T1 tumor model (Fig. 7c). They then evaluated the killing performance of PVP-TiN nanodots on 4T1 cells under NIR or US irradiation and combined NIR and US irradiation. For the *in vitro* cell therapy experiments, the following eight groups were formed: (1) control; (2) US; (3) NIR; (4) US + NIR; (5) PVP-TiN; (6) PVP-TiN + NIR (PTT group); (7) PVP-TiN + US (SDT group); (8) PVP-TiN + NIR + US (PTT–SDT group). It can be seen that the relative cell survival rate in groups (1)–(5) is more than 90%, indicating that US and/or NIR laser irradiation alone does not cause damage to 4T1 cells. However, in the presence of PVP-TiN nanodots in combination with NIR laser irradiation, US irradiation and NIR laser irradiation + US irradiation, the relative cell survival rates in the corresponding groups (6)–(8) were 68.46%, 41.03% and 7.78%, respectively (Fig. 7e). These results show that the therapeutic effect of PVP-TiN is significantly enhanced in the PTT–SDT combination group. This indicates that the therapeutic effect of PVP-TiN nanodots is mainly due to the SDT properties and the combined PTT–SDT treatment can produce a significant synergistic effect. In the *in vivo* experiments, all mice were randomly divided into the following six groups: (1) control; (2) NIR + US; (3) PVP-TiN nanorods; (4) PVP-TiN + NIR (PTT group); (5) PVP-TiN nanorods + US (SDT group); (6) PVP-TiN + NIR + US (PTT + SDT group). Tumors were treated with 1064 nm laser irradiation followed by 2 hours of US irradiation 8 hours after intravenous injection of PVP-TiN nanodots. Tumor growth in mice was monitored after treatment. In the control group, tumors grew rapidly, and neither injection of PVP-TiN nanodots alone nor NIR/US treatment in mice injected with saline showed any inhibitory effect on tumors compared to the control group. Both the PTT group (PVP-TiN + NIR) and the SDT group (TiN + US) showed some inhibition of tumors in the mice, suggesting that the PVP-TiN nanodots have excellent photothermal and acoustic properties. In the PTT + SDT group (PVP-TiN + NIR + US), the tumor growth of the mice was significantly inhibited and the therapeutic performance was much better than that of the SDT group (TiN + US) and the PTT group (PVP-TiN + NIR) (Fig. 7f). Both *in vitro* and *in vivo* evaluations showed high synergistic performance of the PTT–SDT combination treatment, which significantly inhibited tumor growth. This study highlights that TiN nanodots can be used as a novel acoustic sensitizer for improved acoustic dynamics in cancer treatment and expand the application of metal nitrides in cancer imaging and therapy.

3.2.2 Manganese-based materials. In addition to titanium-based sonosensitizers, other transition metal oxides have also attracted research attention to developing sonosensitizers with better therapeutic effects for SDT. Manganese-based nanomaterials (MnO_2, MnO, MnO_x) have shown great potential for application in SDT. Manganese-based nanomaterials offer significant advantages for SDT due to their unique properties, such as good biocompatibility, bioactivity, magnetic properties, and high catalytic activity and stability.[87] Their narrow bandwidth can be easily excited by the US to generate e^- and h^+, which can interact with O_2 or H_2O substrates to promote ROS generation and effectively enhance the effect of SDT in the treatment of tumors.[88] In SDT, manganese-based nanomaterials can be used as efficient sonosensitizers. Zhang *et al.*[89] reported that manganese carbonate ($MnCO_3$) NPs exhibit excellent acoustic dynamic properties. Under ultrasonic conditions, $MnCO_3$NPs[90] can generate $\cdot OH$ and $^1O_2$, which are reactive oxygen species with a strong killing effect on tumor cells. In addition, $MnCO_3$NPs respond to pH and are degraded in acidic microenvironments, releasing CO_2 and Mn^{2+}. Among them, CO_2 bubbles enhanced the cavitation effect under ultrasound, which caused irreversible necrosis of cancer cells and enabled ultrasound imaging. On the other hand, the release of Mn^{2+} can trigger apoptosis in cancer cells by causing mitochondrial dysfunction.[72] *In vivo* experiments have shown that $MnCO_3$NPs induce some tumor inhibition on their own and that their tumor inhibition efficiency is significantly enhanced after ultrasound stimulation. As a non-invasive therapeutic modality, US-induced SDT has been reported to combine sonosensitizers, US sources and O_2 to generate ROS that kill cancer cells, thereby triggering immunogenic cell death (ICD) and activating anti-tumor immunity in cancer cells.[91] Zhan *et al.*[92] have developed a platform to address the limitations of current tumor treatment methods. They integrated SDT with nanovaccines using a porphyrin-based Mn-MOF that has catalase-like and glutathione-lowering properties.[93] This platform aims to overcome challenges such as insufficient targeting of sensitizers to tumors, inappropriate tumor microenvironment conditions like hypoxia and high glutathione, and the lack of effective immune adjuvants leading to low immune responses. The researchers propose using biomimetic nanoparticles based on cancer cell membranes (CM) as drug carriers due to their biocompatibility, prolonged blood circulation, and excellent tumor targeting

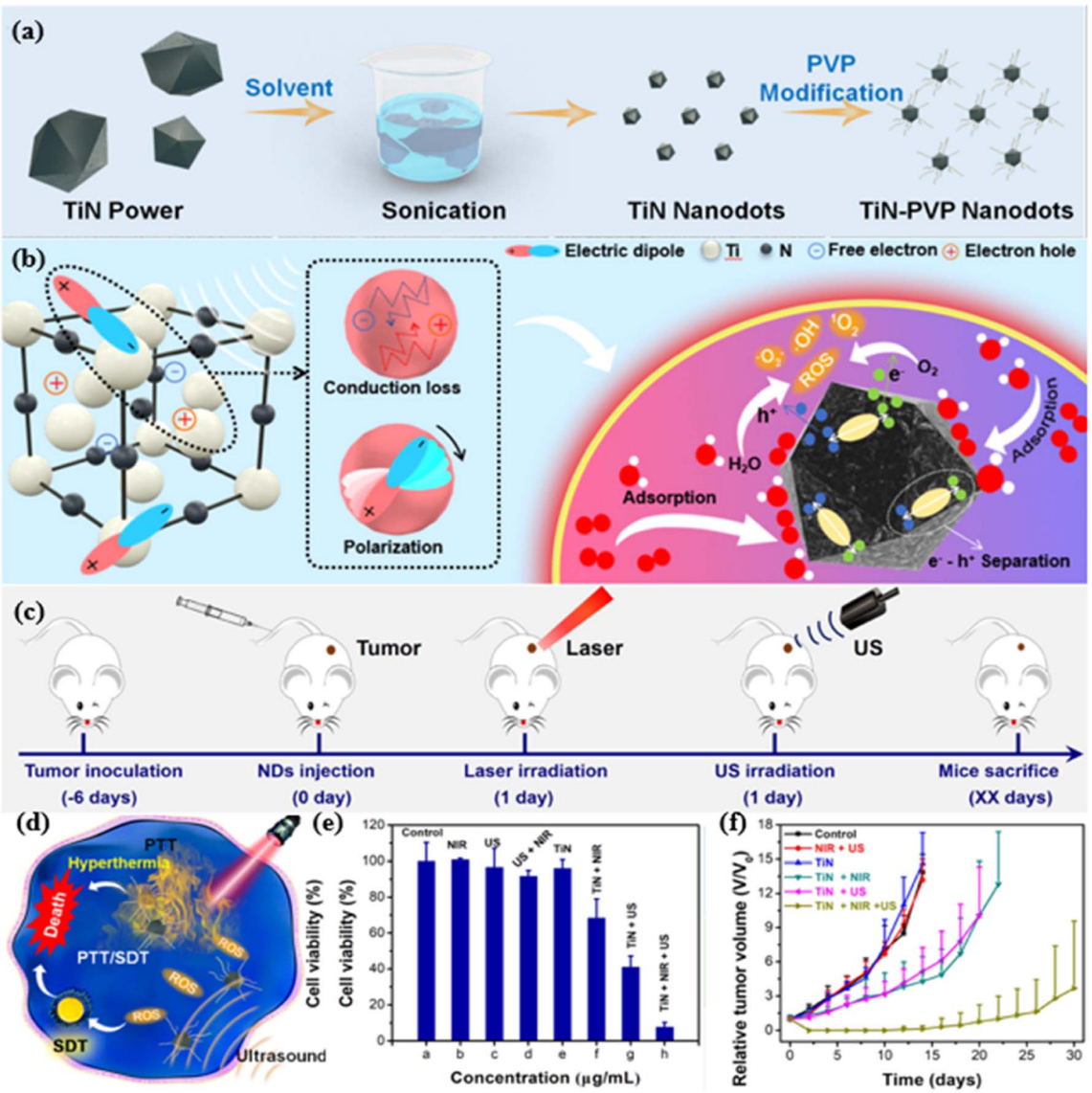

Fig. 7 (a) Schematic preparation and modification of TiN nanodots; (b) TiN nanodots prepared by liquid stripping method for photothermal enhancement of SDT in cancer; (c) TiN nanodot-mediated PTT–SDT in 4T1 tumor model; (d) schematic representation of PVP-TiN nanodots used for mild PTT-enhancement of PTT in cancer cells; (e) 4T1 cells treated with different treatments (control, NIR, US, US + NIR, PVP-TiN, PVP-TiN + NIR, PVP-TiN + US, and PVP-TiN + NIR + US); (f) relative cell survival after various treatments (control, NIR + US, PVP-TiN, PVP-TiN + NIR, PVP-TiN + US, and PVP TiN + NIR + US) after the average tumor growth curves of mice. Copyright 2021, Elsevier.[81]

ability. By combining these approaches, the platform shows promise for effectively treating tumors,[94] especially those in hypoxic conditions. Here, a Mn-MOF-based biomimetic nanoplatform, cMn-MOF@CM,[95] was constructed by electrostatically attractively binding Mn-MOF to CpG oligodeoxynucleotides, an agonist of Toll-like receptor 9 (TLR9), which acts as an immune adjuvant, and then encapsulated with CM derived from B16 murine melanoma cells overexpressing ovalbumin (OVA) antigen (Fig. 8a). The cMn-MOF@CM possessed the characteristics of prolonged blood circulation and enhanced tumor targeting, which effectively reduced tumor hypoxia, decreased intracellular GSH, and induced a strong SDT effect and immunogenic cell death. cMn-MOF@CM in combination with the adjuvant CpG induced ICD and subsequent DC maturation and T cell activation. Meanwhile, cMn-MOF@CM can again be used as a nanovaccine to directly induce DC maturation and T cell activation using OVA as antigen and CpG as adjuvant (Fig. 8b). To determine whether cMn-MOF@CM could effectively reduce the GSH concentration after GSH incubation, cMn-MOF@CM was tested with the GSH kit (Fig. 8c). The ROS-generating ability of cMn-MOF@CM was demonstrated by US irradiation in a hypoxic environment with or without the addition of H_2O_2. The results showed that cMn-MOF@CM did not generate ROS in the absence of H_2O_2. However, the addition of H_2O_2 in the presence of H_2O_2 significantly increased cMn-MOF@CM-induced ROS generation (Fig. 8d), indicates that cMn-MOF@CM was able to produce a good SDT effect even under hypoxic conditions. cMn-MOF@CM exhibited a strong US

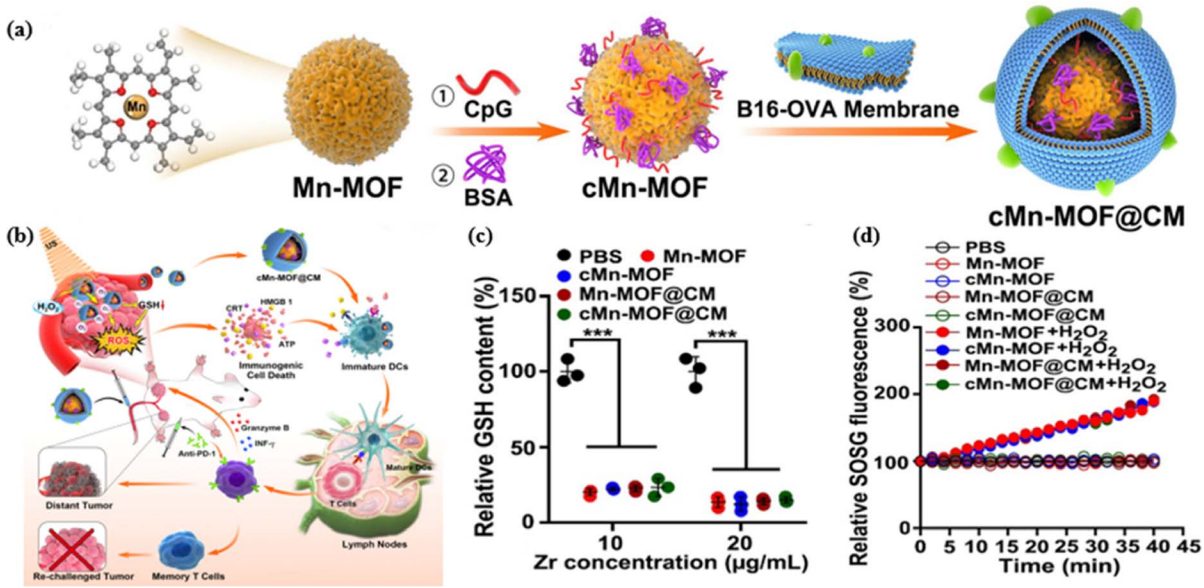

Fig. 8 (a) Schematic preparation of cMn-MOF@CM; (b) schematic representation of cMn-MOF@CM-triggered SDT and nanovaccines for improving anti-PD-1 potency; (c) PBS, Mn-MOF, cMn-MOF, Mn-MOF@CM, and cMn-MOF@CM at Zr concentrations of 10 and 20 μg mL^{-1} together with 5 μM GSH GSH content after 40 min of incubation; (d) ROS generation by PBS, Mn-MOF, cMn-MOF, Mn-MOF@CM and cMn-MOF@CM at a Zr concentration of 10 μg mL^{-1} after US irradiation under low oxygen conditions with or without treatment for different time intervals (1 MHz, 0.9 W cm^{-2}, 30% duty cycle). Copyright 2021, Elsevier.[92]

irradiation systemic anti-tumor immune response and is a potential candidate to improve ICB therapy in the treatment of hypoxic cancer. These results suggest that cMn-MOF@CM in combination with US irradiation may be a potential candidate for improved ICB therapy for the treatment of hypoxic cancer.

3.2.3 Other transition metal-based materials. In addition to common Ti-based and Mn-based sonosensitizers, transition metal oxide-based nanomaterials, such as Zn, Bi, Fe, and Ce-based nanomaterials, have been further broadened as inorganic sonosensitizers for the application of SDT.

Zn-based nanomaterials, such as ZnO, have unique physicochemical properties and good biocompatibility. In SDT, Zn-based nanomaterials can generate ROS through surface effects, quantum size effects, *etc.*, and produce killing effects on tumor cells. In addition, Zn-based nanomaterials can synergistically enhance the therapeutic effect of SDT by modulating the tumor microenvironment and enhancing the immune response. For example, Hu *et al.*[96] designed a zinc oxide nanoacoustic sensitizer co-doped with Fe and Mn to improve the anti-tumor efficiency of SDT by inducing multiple iron apoptosis in tumor cells. Doping the Fe/Mn component into the nanostructure of the ZnO nanosensitizer[97] (Fig. 9a) not only catalyzed the Fenton reaction to generate ROS in the tumor microenvironment with hydrogen peroxide overexpression, but also decreased intracellular glutathione to inhibit ROS degradation.[88] To verify whether D-ZnO-PEG was able to undergo the Fenton reaction, 3,3,5,5-tetramethylbenzidine (TMB) was used as a probe for ·OH. In brief, TMB and 0.1 mM H_2O_2 were mixed with different solution groups (control, US, D-ZnO-PEG, D-ZnO-PEG + US) and then the characteristic peaks were recorded at 650 nm. The results showed that the D-ZnO-PEG groups exhibited a significant increase in intensity, indicating that the doped Fe/Mn underwent a Fenton reaction in the ZnO NPs (Fig. 9b). To investigate the potential mechanism by which iron oxidation enhances the SDT effect, GSH loss was detected using UV spectroscopy. It is shown that the D-ZnO-PEG + US group has a higher GSH consumption than the ZnO-PEG + US group due to the Fe/Mn reference. When irradiated with US, GSH was further oxidized by US-triggered ROS during SDT. It was clearly observed that the D-ZnO-PEG + US group caused a higher degree of GSH degradation[98] than the D-ZnO-PEG group (Fig. 9c). The therapeutic effect of SDT on tumors is enhanced by the development of a unique Fe/Mn-doped ZnO nanosensitizer that simultaneously induces multiple apoptotic effects of iron in a specific tumor microenvironment. This study provides a unique paradigm for improving the SDT performance of nanoscale sensitizers by doping with transition metals and provides important information for further exploration of other efficient nanotherapeutic tumor modalities based on iron death[99] and SDT to achieve highly potent therapeutic effects on tumors.

Bismuth oxide is a non-toxic and chemically stable material that forms the basis for its use in biomedical applications. Although there are relatively few direct studies on the use of bismuth oxide as an acoustic sensitizer for SDT, bismuth oxide has certain similarities with TiO_2 in terms of chemical structure, and therefore it is speculated that bismuth oxide can also be used as an acoustic sensitizer for SDT to treat tumors. For example, the integration of noble metal nanoparticles or the introduction of oxygen defects could further improve the efficacy of bismuth oxide in SDT. Chen *et al.*[100] designed a polymer-modified metal–semiconductor Schottky heterostructure

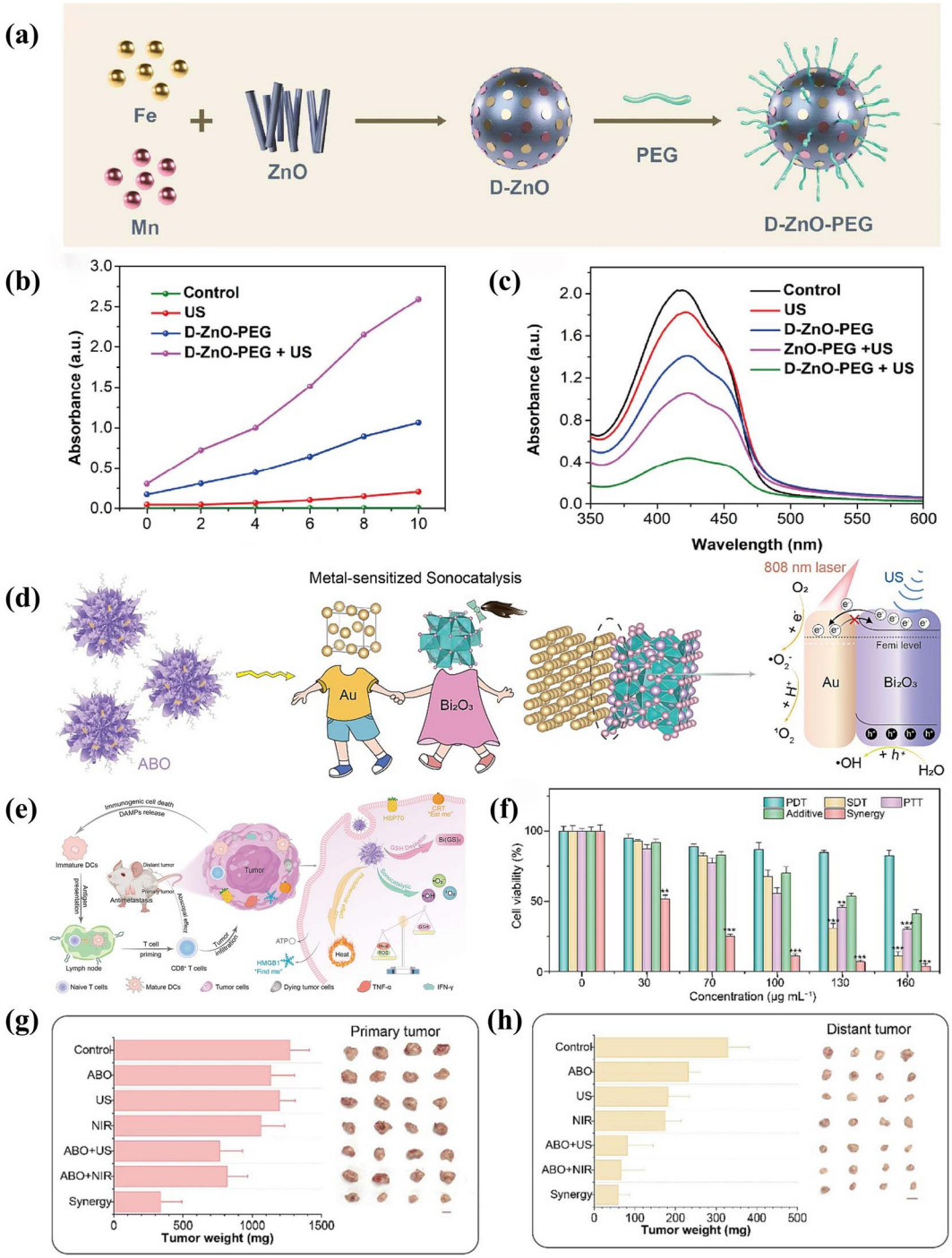

Fig. 9 (a) Schematic preparation of D-ZnO-PEG NPs; (b) characteristic peaks of TMB oxidation of control, US, D-ZnO-PEG and D-ZnO-PEG + US groups over time; (c) comparison of GSH depletion in control, US, D-ZnO-PEG and D-ZnO-PEG + US groups; Copyright 2022, Elsevier.[96] (d) Mechanism of ROS generation by ultrasound-catalyzed ABO nanocatalysts; (e) schematic diagram process of ICD induction in tumor cells by ultrasound-catalyzed ABO nanocatalysts; (f) relative viability of 4T1 cells after different treatments; (g) weights of primary and (h) distal tumors and photos of the corresponding tumors after 14 days of treatment (scale bar = 1 cm). Copyright 2024, Elsevier.[100]

nanocomposite (ABO) as a therapeutic nano platform for inducing ICD (Fig. 9d). In this catalytic system, electrons generated by ultrasonic excitation could be transported from the surface of Bi_2O_3 (BO) semiconductors to Au nanorods (Au NRs) *via* Schottky junctions, and the energy bands effectively prevented the electron backflow.[101] Meanwhile, the synergistic effect of Bi_2O_3 semiconductor and GSH exacerbated the oxidative stress of TME. In addition, the Au NRs exhibited significant photothermal conversion efficiency under 808 nm laser irradiation. Thus, under ultrasound and near-infrared (NIR) light irradiation, ABO nanocomposites activated the ICD in tumor cells, which then synergistically disrupted the tumor's oxidative

stress defense system by GSH depletion, reversed the immunosuppressed TME, and inhibited tumor progression (Fig. 9e). In the *in vitro* study, the therapeutic effect of the synergistic group was approximately 7 times that of the additive group at an ABO concentration of 100 μg mL^{-1}. This result indicated that ultrasound and laser irradiation greatly enhanced the therapeutic effect of ABO, and its synergistic effect was far superior to the purely additive effect, suggesting that the tumor therapeutic effect could be greatly enhanced under US and NIR irradiation (Fig. 9f). In the *in vivo* treatment, the tumor-bearing mice were randomly divided into seven groups: control, ABO, NIR, US, ABO + NIR, ABO + US, and Synergy. Subsequently, the mice in the seven groups received the corresponding treatments. Compared with the control group, the ABO, NIR, and US groups had little effect on tumor growth. In contrast, primary and distal tumors were significantly inhibited in the ABO + NIR, ABO + US, and synergy groups (Fig. 9g and f). In *in vitro* and *in vivo* studies, the nano-acoustic catalytic system exhibited strong reactive oxygen species generation and photothermal properties and synergistically triggered the ICD of tumor cells to inhibit tumor progression, which effectively improved the effectiveness of tumor therapy.

Fe_3O_4 has received increasing attention in the field of SDT due to its superparamagnetism, Fenton-like reactivity and peroxidase-like activity.[102] In the biomedical field, Fe_3O_4 can be used as a magnetic carrier for drug delivery, cell imaging and biosensing, *etc.* Fe_3O_4 has Fenton-like reactivity. It can catalyze the decomposition of H_2O_2 to generate ROS with strong oxidative properties, such as ·OH, under certain conditions. In tumor immunotherapy, Fe_3O_4 nanoparticles are often designed to generate ROS *via* the Fenton reaction in response to the specific characteristics of the tumor microenvironment (*e.g.* low pH, high H_2O_2, *etc.*), thereby eliminating cancer cells. This Fenton-like reactivity provides a broad prospect for the application of Fe_3O_4 in fields such as cancer therapy and environmental protection. In addition to the Fenton-like reactivity, Fe_3O_4 also has the activity of mimicking catalase. Hydrogen peroxidase is an enzyme that catalyzes the decomposition of H_2O_2 to produce O_2 and H_2O, and Fe_3O_4 nano-enzymes can mimic the activity of this enzyme to catalyze the decomposition of H_2O_2 to produce O_2. This mimicry of peroxidase activity makes Fe_3O_4 potentially valuable for biomedical applications. For example, Chen *et al.*[103] reported a tumor-targeted biomimetic acoustic sensitizer-conjugated Fe_3O_4 nanocatalyst combined with CDT and SDT for the treatment of colorectal cancer. They synthesized bovine serum albumin (BSA)-modified Fe_3O_4 nanoparticles by alkaline co-precipitation and coupled them with chlorine e6 (Ce6) as an acoustic sensitizer, and then surface camouflaged CT26 cancer cell membranes to construct tumor-targeting mimetic biomimetic nanocatalysts (MBFCs) for homologous targeting of cancer cells (Fig. 10a). The obtained MBFC nanocatalysts possessed strong catalytic ability and efficient acoustic kinetic properties.[104] Under US irradiation, MBFC could generate a large amount of ROS in the tumor microenvironment (Fig. 10b). The high cellular uptake efficiency of MBFC was confirmed by cell internalization experiments due to the cell membrane-mediated homologous targeting mechanism. The iron staining in MBFC-treated cells was much more pronounced than that in BFC-treated cells, which was mainly due to the fact that iron staining in MBFC-treated cells was much more pronounced than that in BFC-treated cells, and the intracellular uptake ability of the nanoparticles was quantitatively investigated through the measurement of iron content. The results showed that the total iron uptake of MBFC-treated cells was 1.03 μg, while the total iron uptake of BFC-treated cells was 0.25 μg, which was 4.1-fold lower than that of MBFC (Fig. 10c). MBFC nanocatalysts were able to achieve the combined effect of CDT and SDT and significantly induced apoptosis in CT26 cells *in vitro*, and the cell viability in the presence of H_2O_2 was lower than that of the group without added H_2O_2 for both the BFC and MBFC treated cells, the cell viability in the presence of H_2O_2 was lower than that of the group without added H_2O_2 (Fig. 10d), demonstrating that CDT has the effect of killing cancer cells. Under US treatment, the cell viability of BFC and MBFC treated cells was significantly reduced compared with that of control cells (Fig. 10e), which was due to the SDT effect. In US treatment, both BFC and MBFC treatment significantly inhibited tumor growth, suggesting that the combined effect of CDT and SDT could improve the anti-tumor effect. According to the experimental results, it is obvious that the relative tumor volume in the MBFC + US group is much smaller than that in the BFC + US group, further confirming that MBFC is superior to BFC in terms of therapeutic effect due to its targeting ability. The relative weight of the tumor gradually decreased (Fig. 10f), which strongly inhibited the growth of CT26 tumors in living mice. The synergistic effect of CDT and SDT achieved by MBFC can kill cancer cells *in vitro* and inhibit the growth of intestinal tumors *in vivo*, providing a tumor-targeted bionic platform for effective tumor therapy.

Cerium oxide (CeO_2) NPs have nano-enzymatic activity, and their excellent photocatalytic properties, antioxidant properties, high stability, and good biocompatibility have led to their widespread use in tumor therapy. CeO_2 NPs can be used as sonosensitizers or in combination with other sonosensitizers to generate free radicals under the action of ultrasound, which in turn kills tumor cells.[105] The presence of hypoxia in tumor microenvironments (TEMs) results in limited therapeutic efficacy of SDT and PDT. Studies have shown that nanomaterials with catalase-like activity can convert H_2O_2 to O_2, which can alleviate hypoxia in TEMs.[106] The enzyme-like activities of CeO_2 NPs mainly include catalase (CAT), peroxidase (POD), and superoxide dismutase (SOD). CeO_2 can improve the tumor microenvironment and enhance the yield and killing effect of ROS through its catalytic properties. Cao *et al.*[107] designed a direct catalytic synthesis of ultrasmall Cu_2O-liganded carbon nitride for multimodal antitumor therapy. They synthesized $Cu_2O@CeO_2$ nanocomposites[108] on a biocompatible CeO_2 substrate by a self-assisted catalytic growth strategy. Cu_2O can catalyze the pyrolysis of dicyandiamide (DCD) to generate carbon nitride, and ultimately ultra-small Cu_2O-liganded carbon nitride (CuO_2-CN_x@CeO_2) was created on a CeO_2 substrate (Fig. 11a). The peroxidase (POD)-like biocatalytic activity of ROS generation was investigated according to the colorimetric method of 3,3,5,5,-TMB. In the presence of H_2O_2,

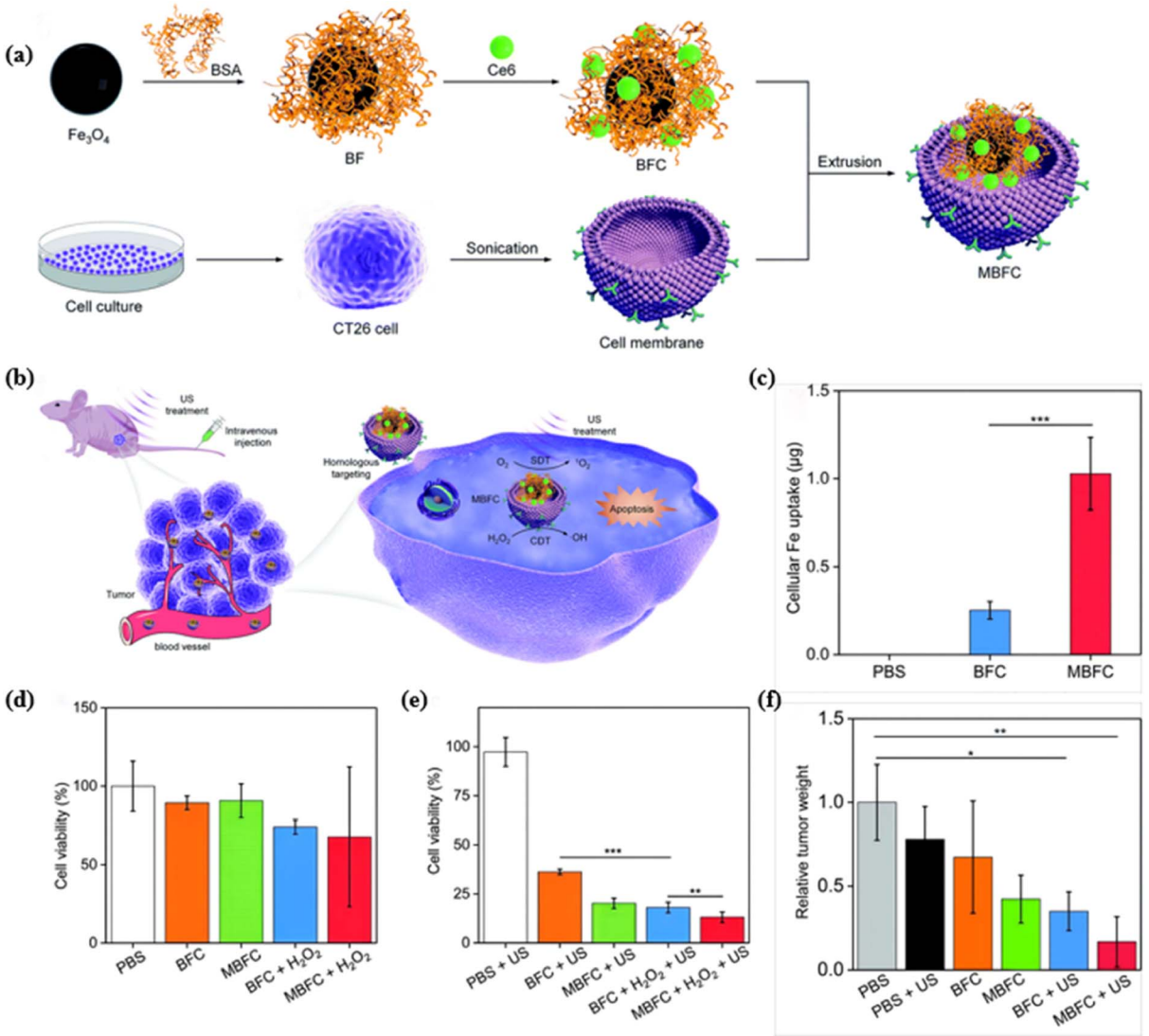

Fig. 10 (a) Schematic illustration of the synthesis of MBFC nanoparticles; (b) schematic illustration of MBFC-mediated targeted combinational CDT/SDT of colon tumors in living mice; (c) quantitative analysis of the cellular uptake of BFC or MBFC nanoparticles by CT26 cells; (d) cell viability of CT26 cells after incubation with BFC or MBFC nanoparticles at the Fe concentration of 50 mg mL^{-1} without or with the addition of H_2O_2 (100 μM); (e) cell viability of CT26 cells after incubation with BFC or MBFC nanoparticles at the Fe concentration of 50 mg mL^{-1} with or without the addition of H_2O_2 (100 μM) and US treatment (1.0 MHz, 1.0 W cm^{-2}). (f) Relative tumor weight in different treatment groups. Copyright 2022, The Royal Society of Chemistry.[103]

Cu_2O-CN_x@CeO_2 could catalyze the oxidation process of TMB to produce blue oxidized TMB (oxTMB) with a characteristic absorbance of 652 nm (Fig. 11b). The experimental results showed that Cu_2O-CN_x@CeO_2 possessed the most excellent peroxidase activity. Cu_2O-CN_x@CeO_2 due to its optimal Cu_2O-CN_x coordination structure and the catalytic activity of CeO_2 as a substrate. Cu_2O-CN_x@CeO_2 not only exhibited highly efficient POD-like activity to generate $-O_2$ (Fig. 11c). and can promote abundant ·OH and $^1O_2$ generation under US irradiation (Fig. 11d). Photoexcitation and ultrasonic radiation have been shown to promote the generation of reactive oxygen species. In an *in vitro* experimental study, the intracellular ROS levels of Cu_2O-CN_x@CeO_2 on B16F10 cells under different treatments were recorded using 2,7-dichlorofluorescein diacetate (DCFH-DA). DCFH-DA reacts with ROS to generate 2,7-dichlorofluorescein (DCF) with green fluorescence. The highest intensity of green fluorescence and the strongest level of ROS generation could be observed in the Cu_2O-CN_x@CeO_2 + US + L group (Fig. 11e). A further process was carried out to examine the biocatalytic killing ability of Cu_2O-CN_x@CeO_2 on B16F10 cells, and the cytotoxicity was detected by CCK8. It could be observed that cell death was most significant in the Cu_2O-CN_x@CeO_2 + US + L group (Fig. 11f). In the *in vivo* experimental study, B16F10 tumor xenografts of Balb/c male mice were used to detect their *in vivo* anti-tumor efficiency. It could be observed that the Cu_2O-CN_x@CeO_2 + US/L group inhibited tumor growth compared with the control group. The Cu_2O-CN_x@CeO_2 + US + L group significantly inhibited tumors with the highest inhibition rate

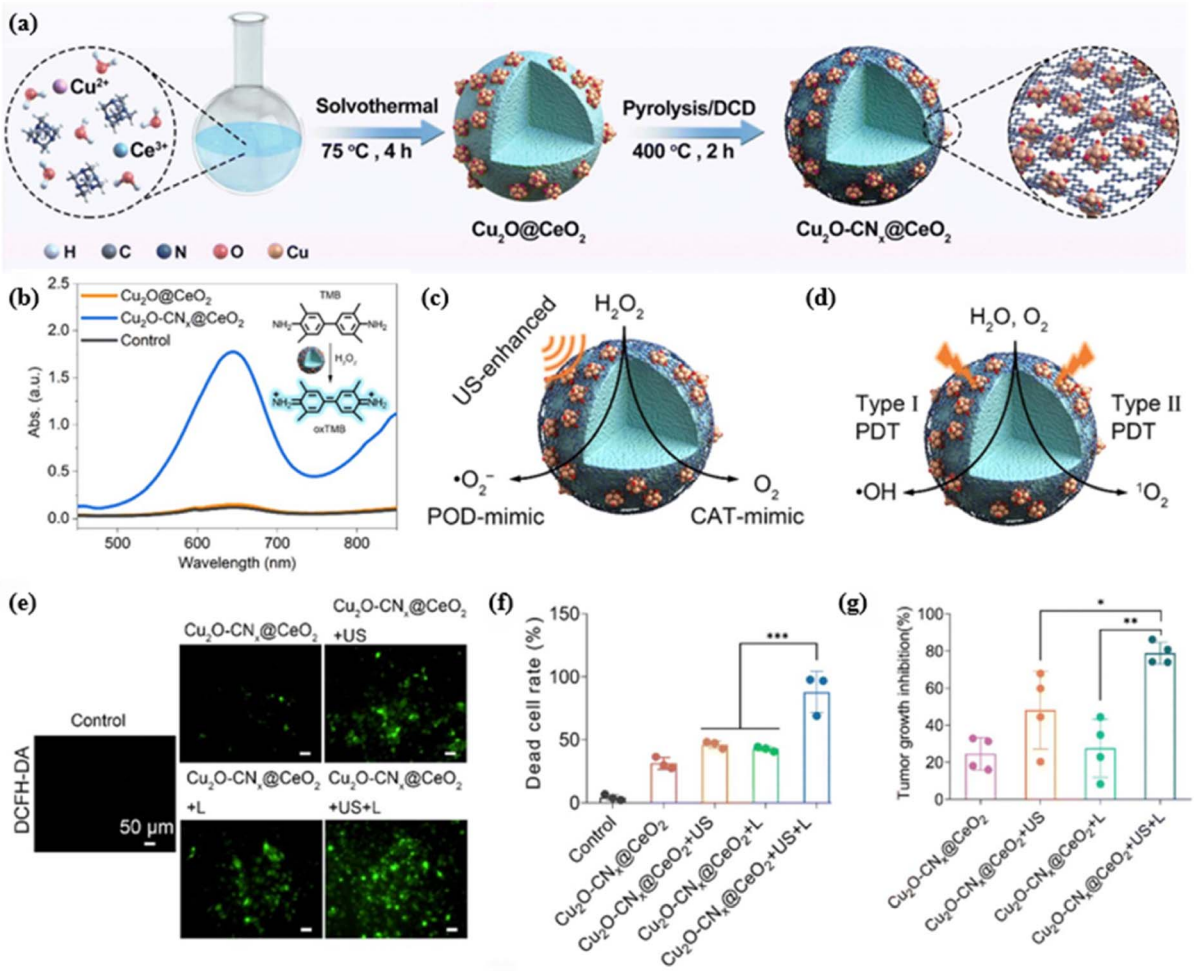

Fig. 11 (a) Illustrated formation procedures for the Cu_2O-CN_x@CeO_2 biocatalyst; (b) UV-vis absorption spectra *via* the TMB method with Cu_2O@CeO_2 and Cu_2O-CN_x@CeO_2; (c) schematic illustration of the CAT-like and ultrasound-enhanced POD-like activity (with H_2O_2); (d) the type I and type II PDT mechanism of Cu_2O-CN_x@CeO_2 (without H_2O_2); (e) fluorescence images of DCFH-DA stained B16F10 cells; (f) quantitative analysis of cell death rate after different treatments; (g) tumor growth inhibition in B16F10 tumors. Copyright 2023, The Royal Society of Chemistry.[107]

of 78.8% (Fig. 11g). The *in vitro* and *in vivo* experiments demonstrated that Cu_2O-CN_x@CeO_2 could effectively inhibit the growth of malignant melanoma through the US/light multimodal antitumor ability. This work provides novel biocatalysts with dual catalytic activities for the generation of ROS and O_2, and offers a new way to engineer multimodal nanoreagents to achieve synergistic inhibition of malignant tumors.

In addition to the Zn, Bi, Fe, and Ce-based materials mentioned above, there are other transition metal oxide-based nanomaterials that may be used as sonosensitizers in SDT. The selection and design of these materials usually depend on factors such as their physicochemical properties, biocompatibility, stability, and ability to generate ROS. The performance of these sonosensitizers can be further optimized and the therapeutic efficacy of SDT can be improved by rational material design and preparation processes. In summary, transition metal oxide-based nanomaterials have a promising application as inorganic sonosensitizers in SDT. However, further studies and explorations on the specific mechanism of action, biosafety, and therapeutic efficacy of these materials are still needed. With the continuous development of nanotechnology and biomedicine, it is believed that more novel and efficient transition metal oxide-based nanomaterials will be developed in the future to provide richer options for SDT.

3.3 Non-metallic acoustic sensitizer

Inorganic non-metallic sonosensitizers are chemical agents consisting of inorganic non-metallic elements that are capable of producing an acoustic dynamic effect in the presence of ultrasound. These elements typically include non-metallic elements such as silicon and carbon, as well as their compounds or nanomaterials. These sonosensitizers usually exhibit superior chemical stability, and low phototoxicity, and are easy to be chemically modified and surface functionalized for modification, thus showing unique advantages in SDT. Under US irradiation, inorganic non-metallic sonosensitizers are able to absorb acoustic energy and undergo separation of

electron–hole pairs. These separated electrons and holes can react with surrounding oxygen or water molecules to generate cytotoxic ROS. These ROS are capable of damaging biomolecules such as cell membranes, DNA and proteins of tumor cells, thus leading to the death of tumor cells.

3.3.1 Si-based materials. Silicon-based nanomaterials have several advantages as sonosensitizers in sound power therapy, and these advantages make them a hot research topic and potential material for clinical applications in this field. Silicon-based nanomaterials have a long cycle time and fewer side effects in living organisms due to their non-toxicity, low immunogenicity and good biocompatibility.[109] This makes them ideal biomedical materials, especially for applications requiring long-term implantation or *in vivo* circulation. Silicon-based nanomaterials can be optimized for acoustic sensitivity by tuning their size, shape and surface properties.[110] This tunability allows researchers to develop nanomaterials with efficient acoustic sensitization properties according to specific therapeutic requirements. Under US irradiation, silicon-based nanomaterials can efficiently generate ROS, such as hydroxyl radicals and superoxide anions. These ROS are strongly oxidative and can damage the biomolecules of tumor cells, such as DNA, proteins, and lipids, thus triggering apoptosis or necrosis of tumor cells. Sun *et al.*[111] prepared SiNWs by thermal evaporation of oxide-assisted growth method and modified SiNWs with Pt nanoparticles by *in situ* reduction method to construct Si–Pt NCs for synergistic PTT-enhanced SDT for the treatment of tumors (Fig. 12a). Due to the good catalytic activity of Pt NPs and the mesoporous structure of SiNWs,[112] the synthesized Si–Pt NCs showed good SDT and CDT activities, which were much stronger than those of pure Pt NPs, and could be used for combined cancer therapy. PTT/SDT/CDT combination therapy has been proven to be an effective method in many aspects. The uniformly dispersed Pt nanoparticles on the surface of SiNW can significantly reduce the bandgap of SiNW from ~1.76 eV bandgap of SiNW to ~0.55 eV bandgap of Si–Pt NC. These results indicate that Si–Pt NCs require lower energy for the excitation of electrons from the valence band (VB) to the conduction band (CB) compared to SiNW. Therefore, it is easier for Si–Pt NCs to improve the separation efficiency of e^-/h^+ under US excitation (Fig. 12b). In addition, the mild photothermal effect could significantly improve the combined SDT & CDT cancer therapy (Fig. 12c). In an *in vitro* experimental study, in order to verify the synergistic therapeutic effect of PTT/SDT/CDT in tumor treatment, it was first verified that the cell viability was found to be unaffected after the addition of H_2O_2. The cell viability was also found to be unaffected after the addition of US, as well as after the addition of 1064 nm laser irradiation alone. Under the assurance of no killing effect on 4T1 cells after addition of H_2O_2/US/1064 nm laser irradiation, the cell viability of the Si–Pt + laser + SDT + H_2O_2 group was found to be lower than that of the Si–Pt + laser + H_2O_2 group and

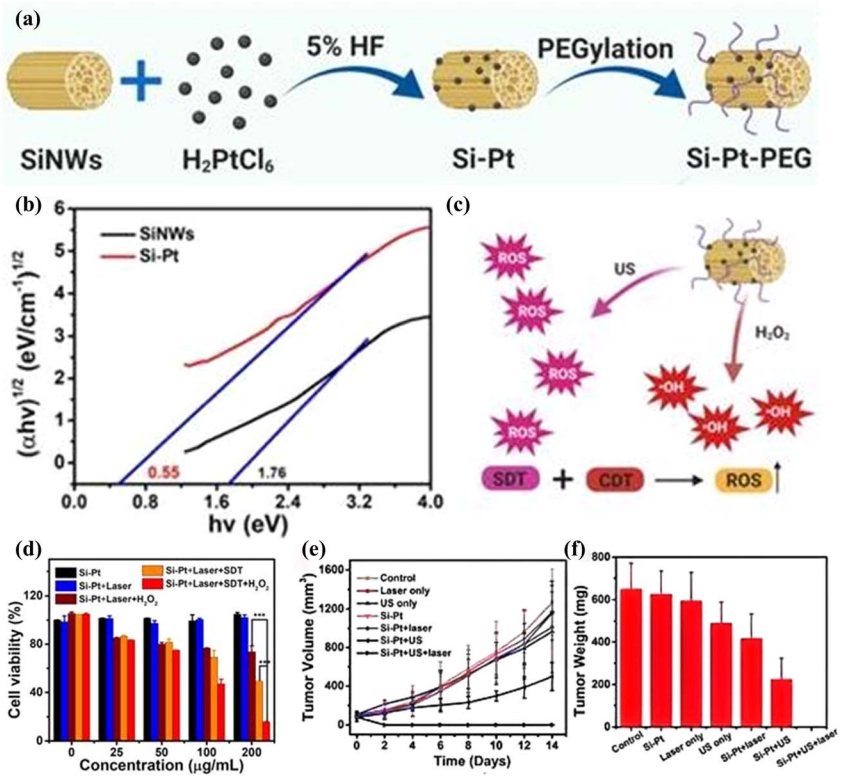

Fig. 12 (a) Schematic illustration of Si–Pt nanocomposites (NCs) with unique photo and ultrasonic properties for photothermal enhanced sonodynamic therapy; (b) the bandgap of SiNWs and Si–Pt NCs; (c) the schematic of sonodynamic and chemodynamic capability of Si–Pt NCs; (d) Si–Pt NCs, 50 μM H_2O_2 and US irradiation in the presence or absence of 1064 nm laser; (e) biodistribution of Si–Pt NCs in mice at different days post-intratumor injection of 4T1 tumor growth curve and (f) tumor weight. Copyright 2021, Ivyspring International.[111]

the Si–Pt + laser + SDT group, which suggests that the mild photothermal effect of Si–Pt nanocrystals enhances their efficacy of CDT and SDT (Fig. 12d). In the *in vivo* experimental study, the changes in tumor volume and weight of mice were recorded under different treatment treatments. It can be seen that the tumor growth in the Si–Pt + US group was significantly inhibited and even disappeared in the synergistic therapy-treated tumors (Fig. 12e and f), while the tumors in the other groups were still growing, which proved that the mild photothermal effect of the enhanced CDT and SDT had a good therapeutic effect on the tumors. Both *in vivo* and *in vitro* experiments demonstrated that Si–Pt nanoparticles could be used for SDT/CDT combination therapy with significant inhibitory effects. Therefore multifunctional Si–Pt NCs have great application significance in novel cancer therapy.

3.3.2 Carbon-based materials. Carbon-based nanomaterials such as graphene, fullerenes, and carbon dots (CDs) are characterized by their unique physicochemical properties,[113,114] in which their internal carbon atoms are arranged in a hexagonal lattice structure with sp^2 hybridization. This special structure endows them with a range of unique chemical and physical properties, which has led to these materials showing great potential for applications in a number of fields, especially in bioimaging, drug delivery, and cancer therapy. Graphene, as a two-dimensional carbon nanomaterial, has excellent electrical conductivity and optical properties, making it a potential candidate for bioimaging. However, relatively little research has been conducted on graphene for direct application in bioimaging, and more often it has been modified or composited with other materials to enhance its biocompatibility and imaging effects. For example, Pan *et al.*[115] designed a novel acoustic sensitizer with both efficient ROS generation and enhanced mechanical effects. In this study, carbon-doped zinc oxide nanoparticles (C–ZnO), achieved both ROS generation and US-induced mechanical effects by introducing C into the conventional inorganic acoustic sensitizer ZnO[116] (Fig. 13a). The unique C-doped structure and O defects effectively prevented the rate of electron–hole complexation by determining and calculating the band gaps of ZnO and C–ZnO. The band gap of ZnO was 3.22 eV, while that of C–ZnO was significantly narrower at 2.75 eV (Fig. 13b). This indicates that C doping effectively reduces the bandgap of ZnO and significantly extends the charge carrier lifetime. In addition, by measuring the mechanical force generated by C–ZnO under US irradiation. The results showed that the specific surface area of ZnO was 16.26 $m^2\ g^{-1}$ and that of C–ZnO was 160.93 $m^2\ g^{-1}$ (Fig. 13c). The significant increase in specific surface area greatly facilitated the generation of ROS and promoted the enhancement of mechanical effects produced under US irradiation. The dual effects of SDT and C–ZnO-mediated mechanotherapy exhibited excellent antitumor efficacy *in vitro* and *in vivo*, along with a high degree of biosafety. This is important for the future development of US-responsive nanomaterials for mechanoacoustic kinetic therapy in cancer treatment.

Specific elements in the fullerene molecule (*e.g.*, Gd) can generate hydrophilic groups to achieve good contrast effects. It has been shown that fullerenes containing Gd perform well in MRI contrast, and their contrast effect is far superior to that of conventional contrast agents. This property makes fullerenes have a broad application prospect in the field of bio-imaging. The

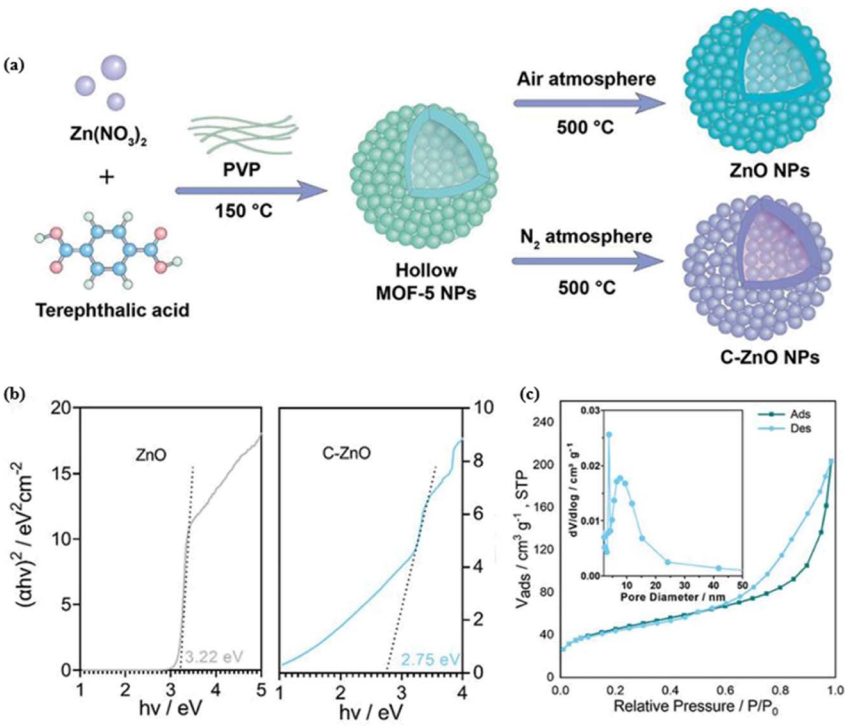

Fig. 13 (a) Synthesis process of ZnO and C–ZnO; (b) optical band gaps of ZnO and C–ZnO; (c) N_2 adsorption–desorption isotherms and pore size distribution of C–ZnO. Copyright 2024, Wiley-VCH.[115]

molecular structure of fullerenes enables them to carry large amounts of therapeutic drugs and has good biocompatibility.[117] Studies have shown that fullerenes can be used as drug delivery carriers to deliver drugs to tumor sites, showing promise in the diagnosis and treatment of tumors. Iwase *et al.*[118] investigated the acoustic kinetics-induced antitumor effects of pyrrolidine-triacontanic acid fullerenes (PTFs). PTFs showed significant ultrasound-induced antitumor effects as well as a significant enhancement of ultrasound-induced cellular damage *in vitro*. PTF increased the rate of ultrasound-induced cell injury in isolated sarcoma 180 cells by approximately 5-fold. Tumor tissue destruction was observed in the combination of PTF and US treatment, whereas neither PTF alone nor ultrasound alone induced necrosis. The above results demonstrated that PTF showed excellent US-induced antitumor effects.

CDs are an emerging class of zero-dimensional fluorescent carbon nanomaterials with small highly carbonized cores and polymer surface groups. Their unique structure endows CDs with excellent optical and electronic properties, making them a preferred material in the field of bioimaging. The imaging function of CDs stems from their unique optical features or functional reagents bound to their cores or surfaces, which enable imaging at the cellular or even single-molecule level. CDs are characterized by low toxicity, high chemical stability, excellent water-solubility, and good biocompatibility.[119] These properties make CDs promising for drug delivery applications. The tunable functional properties of CDs make them ideal nanocapsules and nanocarriers[120] for loading and delivering drugs and genes to specific targets in the body. Recently, iron-doped multivalent manganese oxide nanoparticles (FDMNs) studied by Sun *et al.*[121] have been well applied as sonosensitizers in SDT for tumor therapy. Due to the presence of oxygen vacancies, a large number of oxygen molecules adsorbed on the surface of FDMNs can enter the tumor microenvironment, effectively preventing ultrasound-triggered electron–hole pair recombination and generating a large number of ROS for SDT tumor therapy. Based on the study of FDMNs for SDT tumor therapy, Cheng *et al.*[122] designed a novel acoustic sensitizer synthesized with Cu–CDs (Fig. 14a) for the acoustic kinetic therapy of glioblastoma multiforme (GBM) (Fig. 14b). The Cu–CDs have unique p–n junctions and abnormally narrow bandgaps, and Cu referencing converts the CDs into a 1.58 eV

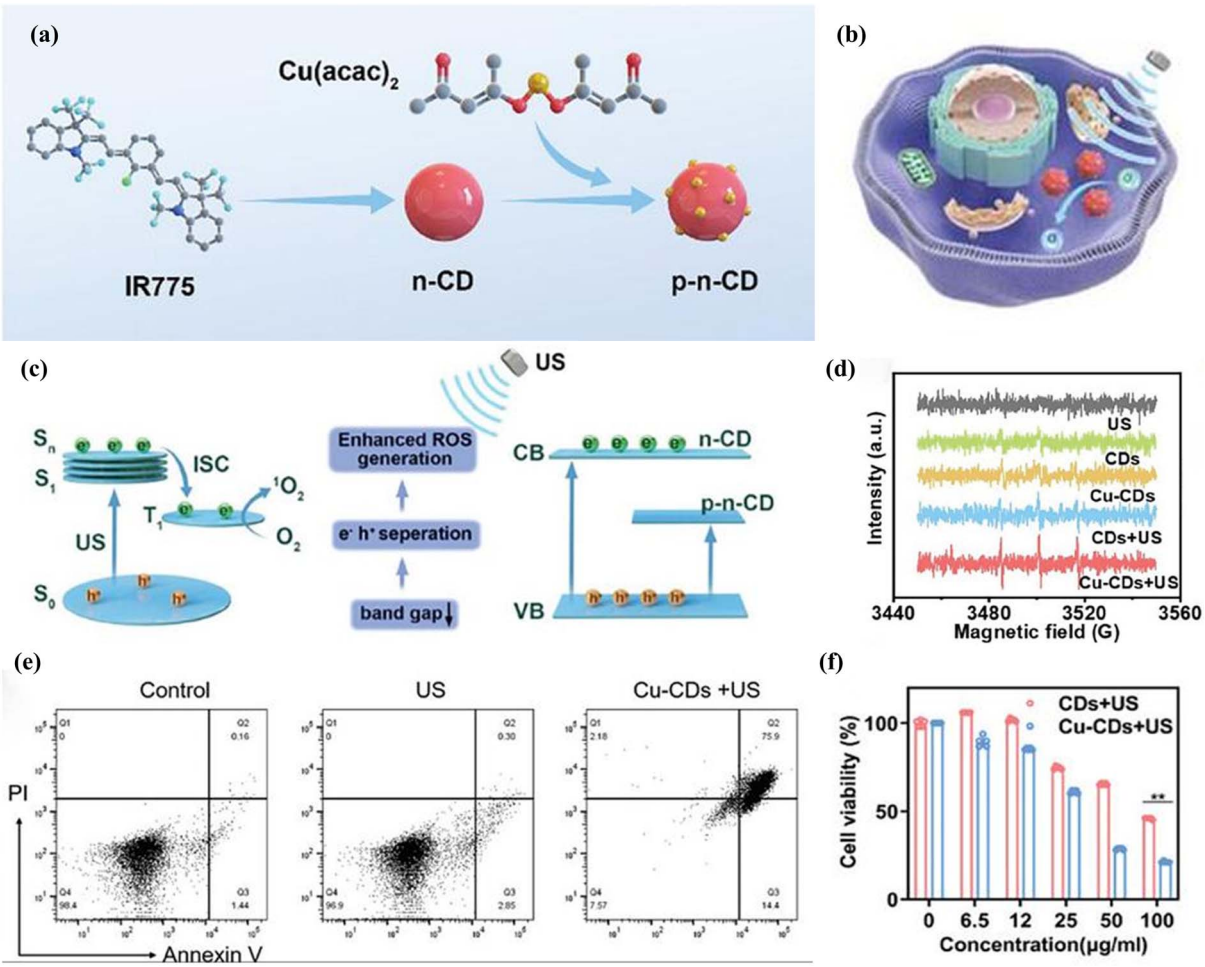

Fig. 14 (a) Design and mechanism of Cu–CDs for sonodynamic cancer therapy; (b) mechanisms of Cu–CDs for acoustic power cancer therapy; (c) schematic diagram of $^1O_2$ generation mechanisms of Cu–CDs; (d) ESR spectra of US-triggered $^1O_2$ generation using TEMP as the trapping agent for $^1O_2$; (e) flow cytometry analysis of U87 cells after different treatments stained with annexin V-FITC/PI; (f) relative cell viability of U87 cells incubated with CDs and Cu–CDs + US (1.0 w cm^{-2}). Copyright 2024, Wiley-VCH.[122]

Table 1 Comparative analysis of inorganic sonosensitizers

Material class	Stability	Biocompatibility	ROS yield	Key limitations
Noble metals	High	Excellent	Moderate	High cost, limited depth penetration
Transition metals	pH-dependent	Good	High	GSH sensitivity
Non-metallic	Ultra-high	Variable	Low	Poor tumor targeting

bandgap p–n semiconductors, resulting in improved separation efficiency of electrons and holes and improved ROS generation. The p–n-CD acoustic sensitizer acts as a US transducer, which can generate $^1O_2$ through the energy transfer and SDT mechanisms. Briefly, due to the small band gap, when p–n-CDs undergo rapid separation of surface charges and holes under US irradiation, the separated electrons absorb energy from the ground state (S_0) to jump to a single-line excited state (S_1). A portion of this absorbed energy is released through the interlinear crossover to form a triplet excited state (T_1). p–n-CD triplet state's relatively long half-life (10.7 μs) permits efficient energy transfer to nearby oxygen molecules, which results in the production of $^1O_2$ *via* the type II pathway (Fig. 14c). Consequently, this process destroys cells in the surrounding region, ultimately leading to cell death. This is the mechanism by which ROS generation by carbon-based sonosensitizers induces tumor cell death. By using 2,2,6,6-tetramethylpiperidine (TEMP) as a trapping agent for $^1O_2$, electron spin resonance (ESR) spectra were recorded (Fig. 14d). The results showed that "Cu–CDs + US" produced significantly stronger ESR signals, indicating enhanced $^1O_2$ production. In addition, the introduction of copper doping induced copper body deposition, and Cu–CDs induced a biological reaction leading to cell death called copper death. Specifically, Cu–CDs efficiently bound to lipoylated mitochondrial enzymes and induced the aggregation of lipoylated dihydrosulfonyltransacetylase (DLAT), leading to copper conversion. The copper death mechanism further amplified the effects of SDT, leading to more potent therapeutic outcomes compared to SDT alone. In cellular *in vitro* assays, to determine the *in vitro* SDT performance of Cu–CDs on U87 cells, 5 min of US irradiation at 1.0 w cm^{-2} was performed. Under the same concentration (50 μg ml^{-1}) and US irradiation conditions, the cell survival of different treatment groups (US, CDs, Cu–CDs, CDs + US and Cu–CDs + US) were compared relative to the control group for 24 h. The SDT effect was greatest in the Cu–CD + US group (Fig. 14f). Flow cytometry analysis supported the WST-1 results and live/dead cell analysis, and Cu–CDs showed that US enhanced ROS generation and tumor death (Fig. 14e). The proportion of late apoptotic cells was higher in the US-enhanced Cu–CDs group (75.9%). Cu–CDs effectively inhibited the growth of glioblastoma tumors and prolonged the survival of mice with these tumors. This study provides support for the application of carbon-based nanomaterials as ultrasound sensitizers in tumor therapy.

3.4 Stability, biocompatibility, and metabolic pathways of inorganic sonosensitizers

To systematically evaluate the performance of inorganic sonosensitizers in sonodynamic therapy (SDT), we conducted a comparative analysis of three primary material classes: noble metals (Au, Ag, Pt), transition metal oxides (*e.g.*, MnO_2), and carbon-based nanomaterials. This assessment focuses on critical parameters including stability, biocompatibility, reactive oxygen species (ROS) yield, and practical limitations (Table 1). Noble metal-based sonosensitizers exhibit high structural stability and excellent biocompatibility, yet their moderate ROS generation efficiency is constrained by high production costs and limited tissue penetration depth. Transition metal oxides, represented by MnO_2, demonstrate pH-dependent stability and superior ROS yields *via* Fenton-like reactions; however, their efficacy is compromised by glutathione (GSH) scavenging in the tumor microenvironment. Carbon-based materials, while achieving ultra-high stability, suffer from inconsistent biocompatibility (dependent on surface functionalization) and low ROS productivity, alongside poor tumor-targeting specificity. This comparative framework underscores the necessity of balancing material properties with clinical requirements, guiding the rational selection and optimization of sonosensitizers for SDT applications.

The clinical translation of inorganic sonosensitizers necessitates rigorous evaluation of their biosafety. Noble metal-based nanoparticles (*e.g.*, Au, Ag) exhibit excellent biocompatibility but face challenges in long-term accumulation due to slow renal clearance. Recent studies suggest that sub-5 nm Au nanoparticles can enhance urinary excretion. Transition metal oxides (*e.g.*, MnO_2) are degradable in acidic TME *via* Mn^{2+}/Mn^{4+} redox cycles, yet excessive Mn^{2+} may induce neurotoxicity. Silicon-based materials, while biodegradable into orthosilicic acid ($Si(OH)_4$), require precise size control (<10 nm) to avoid pulmonary inflammation. Carbon-based sonosensitizers (*e.g.*, graphene quantum dots) show pH-dependent degradation but raise concerns about prolonged retention in reticuloendothelial systems. Future studies should prioritize real-time tracking of sonosensitizer metabolism using isotopic labeling (*e.g.*, ^{64}Cu-labeled probes).

4 Conclusion and outlook

With the booming of nanomedicine technology, the research on sonosensitizers at the core of SDT, an emerging cancer treatment, is experiencing an unprecedented boom in exploration. In this in-depth review, our attention is focused on the key area of inorganic sonosensitizers, especially precious metals (*e.g.*, Au, Ag, Pt): these metals are used in SDT mainly due to their unique photovoltaic properties and stability. However, they are costly and may trigger an immune response in some cases. Therefore, future research should focus on the development of more cost-effective and biocompatible precious metal

nanostructures; transition metals (*e.g.*, Ti, Mn, *etc.*): the tunable redox activity of these metals offers new possibilities for SDT, while their biosafety and long-term effects still need to be further evaluated. By precisely controlling the size, shape and surface chemistry of the nanoparticles, their biodistribution and clearance mechanisms can be optimized; other metals (*e.g.*, Zn, Bi, Fe, and Ce, *etc.*): these metals have attracted much attention due to their good catalytic activity. However, their biocompatibility and stability still need to be further verified. Their SDT performance can be improved by composite or surface modification with other materials; silicon-based materials are ideal candidates for SDT due to their good biocompatibility and redox activity, but their mechanical strength and long-term stability still need to be improved. Their SDT effect can be enhanced by introducing functionalized groups or constructing composite structures; carbon-based materials, such as graphene, fullerenes and carbon dots, are popular for their excellent conductivity and biocompatibility. Whereas, their biodistribution and clearance mechanisms still need to be thoroughly investigated. Their SDT performance can be improved by precisely controlling the size and shape of the materials and introducing targeting groups.

We not only comprehensively review the basic mechanism of action of SDT, the direct killing of cancer cells by ROS or physical effects generated by the interaction of ultrasound and sonosensitizers – but also analyze in depth a variety of cutting-edge strategies aimed at enhancing the efficacy of SDT. These strategies cover: (1) material design and cavitation effect: by designing nanoparticles with specific shapes and structures, the cavitation effect can be enhanced, thereby improving the efficiency of ultrasound energy delivery and utilization in tumor tissues. For example, the use of nanoparticles with a porous structure can increase the scattering and absorption of ultrasound; (2) metal coupling and multifunctional nanoplatforms: through metal coupling technology, multifunctional nanoplatforms can be constructed to enhance the stability of the sonosensitizers, as well as to facilitate the subsequent biomodification and targeted delivery. This strategy can significantly improve the specificity and therapeutic efficacy of SDT; (3) defect engineering and energy band structure modulation: through the implementation of defect engineering, it is possible to modulate the energy band structure of the sonosensitizers and optimize their response performance to ultrasound. This strategy can significantly improve the efficiency and sensitivity of SDT; (4) material modification and conductivity enhancement: increasing conductivity through material modification can promote the electron transfer process and accelerate the generation of ROS. This strategy can significantly improve the killing effect of SDT; (5) targeting strategy and tumor microenvironment remodeling: the use of advanced targeting strategies can improve the specific recognition of tumor cells by sonosensitizers. Meanwhile, exploring new ways to remodel the tumor microenvironment, such as improving the oxygen supply and blood circulation inside the tumor, can enhance the therapeutic effect of SDT emerging strategies to enhance SDT include surface engineering of sonosensitizers with tumor-targeting ligands (*e.g.*, anti-EGFR antibodies) and stimuli-responsive coatings.[123] For instance, pH-sensitive polymers could enable site-specific drug release in acidic TME. Combinatorial approaches integrating SDT with immune checkpoint inhibitors (*e.g.*, anti-PD-1) have shown synergistic abscopal effects in recent preclinical trials. Additionally, nanoparticle-mediated sonodynamic-chemo therapy hybrids (*e.g.*, DOX-loaded TiO_2) demonstrate enhanced tumor penetration through ultrasound-triggered cavitation). Multimodal synergistic treatment can be achieved by researching combined treatment modes, combining chemotherapy, radiotherapy and photodynamic therapy; as well as using image-guided technology to achieve precise positioning and real-time monitoring of the SDT process to ensure the safety and effectiveness of the treatment.

However, despite the remarkable progress made by researchers in developing efficient, safe, and biocompatible sonosensitizers, unfortunately, no acoustic sensitizer has yet to successfully cross the laboratory-to-clinical divide and achieve true clinical application. This is mainly due to the fact that there are still many challenges regarding the stability, biodistribution, clearance mechanism, and long-term safety of sonosensitizers *in vivo*.

Future of SDT requires interdisciplinary convergence: (1) material scientists and clinicians should co-design sonosensitizers with real-time imaging capabilities (*e.g.*, US-guided); (2) pharmacologists need to establish standardized protocols for sonosensitizer dosing and US parameter optimization; (3) regulatory frameworks must adapt to assess nanotherapeutic safety in SDT combination regimens. With global initiatives like the International SDT Consortium (2024), clinical trials may soon validate these laboratory breakthroughs.

Data availability

All data have been included in the main text.

Conflicts of interest

There is no conflict to declare.

Acknowledgements

This work was financially supported by the Science and Technology Project of China Minmetals Corporation (2022ZXA02), Shanghai Collaborative Innovation Center of Energy Therapy for Tumors, the Medical-Engineering Interdisciplinary Project of University of Shanghai for Science and Technology (1022310503), Open Research Fund of School of Chemistry and Chemical Engineering, Henan Normal University (2024Y12), the Technical Innovation Team of Henan Normal University (2022TD03). The authors greatly appreciated these supports.

References

1 C. Dong, H. Hu, L. Sun and Y. Chen, *Biomed. Mater.*, 2021, **16**, 032006.

2 U. Anand, A. Dey, A. K. S. Chandel, R. Sanyal, A. Mishra, D. K. Pandey, V. De Falco, A. Upadhyay, R. Kandimalla, A. Chaudhary, J. K. Dhanjal, S. Dewanjee, J. Vallamkondu and J. M. Pérez de la Lastra, *Gene Dis.*, 2023, **10**, 1367–1401.
3 L. Sun, P. Wang, J. Zhang, Y. Sun, S. Sun, M. Xu, L. Zhang, S. Wang, X. Liang and L. Cui, *Biomater. Sci.*, 2021, **9**, 1945–1960.
4 K. D. Miller, L. Nogueira, T. Devasia, A. B. Mariotto, K. R. Yabroff, A. Jemal, J. Kramer and R. L. Siegel, *Ca-Cancer J. Clin.*, 2022, **72**, 409–436.
5 A. R. Lima, L. Santos, M. Correia, P. Soares, M. Sobrinho-Simões, M. Melo and V. Máximo, *Genes*, 2018, **9**, 115.
6 M. Cedzyński and A. S. Świerzko, *Cancers*, 2024, **16**, 3116.
7 L.-L. Bu, J. Yan, Z. Wang, H. Ruan, Q. Chen, V. Gunadhi, R. B. Bell and Z. Gu, *Biomaterials*, 2019, **219**, 119182.
8 F. Peng, J. Liu, J. Chen, W. Wu, Y. Zhang, G. Zhao, Y. Kang, D. Gong, L. He, J. Wang, W. Zhang and F. Qiu, *ACS Nano*, 2023, **17**, 20135–20152.
9 X. Shi and X. Sun, *Cancer Chemother. Pharmacol.*, 2017, **80**, 909–917.
10 M. L. S. Silva, *Int. J. Pharm.*, 2024, **665**, 124685.
11 L. Han, X.-Y. Zhang, Y.-L. Wang, X. Li, X.-H. Yang, M. Huang, K. Hu, L.-H. Li and Y. Wei, *J. Controlled Release*, 2017, **259**, 40–52.
12 N. Yumita, R. Nishigaki, K. Umemura and S.-I. Umemura, *Jpn. J. Cancer Res.*, 1989, **80**, 219–222.
13 J. H. Correia, J. A. Rodrigues, S. Pimenta, T. Dong and Z. Yang, *Pharmaceutics*, 2021, **13**, 1332.
14 X. Song, F. Li, F. Tian, L. Ren, Q. Wang, C. Jiang, T. Yan and S. Zhang, *Acta Biomater.*, 2023, **157**, 538–550.
15 Z. Dai and A. A. Exner, *Bioconjugate Chem.*, 2022, **33**, 991–992.
16 J. Guo, X. Pan, C. Wang and H. Liu, *Bioconjugate Chem.*, 2022, **33**, 993–1010.
17 K. Bian, W. Yang, Y. Xu, W. Zeng, H. Wang, H. Liang, T. Cui, Z. Wang and B. Zhang, *Small*, 2022, **18**, 2202921.
18 A. Radivoievych, S. Prylutska, O. Zolk, U. Ritter, M. Frohme and A. Grebinyk, *Pharmaceutics*, 2023, **15**, 2616.
19 L. Wang, M. Niu, C. Zheng, H. Zhao, X. Niu, L. Li, Y. Hu, Y. Zhang, J. Shi and Z. Zhang, *Adv. Healthcare Mater.*, 2018, **7**, 1800819.
20 X. Wang, Y. Wang, P. Wang, X. Cheng and Q. Liu, *Ultrasonics*, 2011, **51**, 539–546.
21 J. Chen, Q. Zhou and W. Cao, *Adv. Funct. Mater.*, 2024, **34**, 2405844.
22 X. Feng, Y. Shi, L. Xie, K. Zhang, X. Wang, Q. Liu and P. Wang, *J. Med. Chem.*, 2018, **61**, 7189–7201.
23 A. Luiz-Ferreira, T. Pacifico, Á. C. Cruz, F. Laudisi, G. Monteleone and C. Stolfi, *Int. J. Mol. Sci.*, 2023, **24**, 16596.
24 S. Liang, X. Deng, G. Xu, X. Xiao, M. Wang, X. Guo, P. a. Ma, Z. Cheng, D. Zhang and J. Lin, *Adv. Funct. Mater.*, 2020, **30**, 1908598.
25 T. Kasai, K. Miyauchi, N. Yanagisawa, K. Kajimoto, N. Kubota, M. Ogita, S. Tsuboi, A. Amano and H. Daida, *Heart*, 2013, **99**, 22–29.
26 L. Wang, Y. Hu, Y. Hao, L. Li, C. Zheng, H. Zhao, M. Niu, Y. Yin, Z. Zhang and Y. Zhang, *J. Controlled Release*, 2018, **286**, 74–84.
27 J. Bogdan, J. Pławińska-Czarnak and J. Zarzyńska, *Nanoscale Res. Lett.*, 2017, **12**, 225.
28 X. Feng, C. Wu, W. Yang, J. Wu and P. Wang, *Int. J. Mol. Sci.*, 2022, **23**, 7981.
29 S. Yamamoto, M. Ono, E. Yuba and A. Harada, *Nanomaterials*, 2017, **7**, 268.
30 H.-Y. Xia, B.-Y. Li, Y. Zhao, Y.-H. Han, S.-B. Wang, A.-Z. Chen and R. K. Kankala, *Coord. Chem. Rev.*, 2022, **464**, 214540.
31 T. Xu, S. Zhao, C. Lin, X. Zheng and M. Lan, *Nano Res.*, 2020, **13**, 2898–2908.
32 G. Wang, W. Wu, J.-J. Zhu and D. Peng, *Ultrason. Sonochem.*, 2021, **79**, 105781.
33 N. H. Ince, G. Tezcanli, R. K. Belen and I. G. Apikyan, *Appl. Catal., B*, 2001, **29**, 167–176.
34 P. Yan, L.-H. Liu and P. Wang, *ACS Appl. Bio Mater.*, 2020, **3**, 3456–3475.
35 Y. Xin, Z. Guo, A. Ma, E. Shi, Z. Li, Z. Liang, Z. Qian, L. Yang, Y. Wang, M. Cao and X. Yang, *Chem. Eng. J.*, 2023, **451**, 138782.
36 J. An, H. Hong, M. Won, H. Rha, Q. Ding, N. Kang, H. Kang and J. S. Kim, *Chem. Soc. Rev.*, 2023, **52**, 30–46.
37 R. G. Thomas, U. S. Jonnalagadda and J. J. Kwan, *Langmuir*, 2019, **35**, 10106–10115.
38 D. Huang, C. Zhao, B. Wen, X. Fu, L. Shang, W. Kong and Y. Zhao, *Chem. Eng. J.*, 2022, **435**, 134871.
39 X. Wang, X. Zhong, F. Gong, Y. Chao and L. Cheng, *Mater. Horiz.*, 2020, **7**, 2028–2046.
40 P. Xu, C. Wen, C. Gao, H. Liu, Y. Li, X. Guo, X.-C. Shen and H. Liang, *ACS Nano*, 2024, **18**, 713–727.
41 A. Sazgarnia, A. Shanei, A. R. Taheri, N. T. Meibodi, H. Eshghi, N. Attaran and M. M. Shanei, *J. Ultrasound Med.*, 2013, **32**, 475–483.
42 N. S. Abadeer and C. J. Murphy, *J. Phys. Chem. C*, 2016, **120**, 4691–4716.
43 Y. L. Loke, A. Beishenaliev, P.-W. Wang, C.-Y. Lin, C.-Y. Chang, Y. Y. Foo, F. N. Faruqu, B. F. Leo, M. Misran, L. Y. Chung, D.-B. Shieh, L. V. Kiew, C.-C. Chang and Y. Y. Teo, *Ultrason. Sonochem.*, 2023, **96**, 106437.
44 Y. Zhang, Y. Chen, Y. Zhang, H. Cong, B. Fu, S. Wen and S. Ruan, *J. Nanopart. Res.*, 2013, **15**, 2014.
45 H. Hu, J. Zhao, K. Ma, J. Wang, X. Wang, T. Mao, C. Xiang, H. Luo, Y. Cheng, M. Yu, Y. Qin, K. Yang, Q. Li, Y. Sun and S. Wang, *J. Controlled Release*, 2023, **359**, 188–205.
46 B. Geng, S. Zhang, X. Yang, W. Shi, P. Li, D. Pan and L. Shen, *Chem. Eng. J.*, 2022, **435**, 134777.
47 K. Li, C. Lin, M. Li, K. Xu, Y. He, Y. Mao, L. Lu, W. Geng, X. Li, Z. Luo and K. Cai, *ACS Nano*, 2022, **16**, 2381–2398.
48 B. Geng, S. Xu, L. Shen, F. Fang, W. Shi and D. Pan, *Carbon*, 2021, **179**, 493–504.
49 C. Shuai, W. Guo, P. Wu, W. Yang, S. Hu, Y. Xia and P. Feng, *Chem. Eng. J.*, 2018, **347**, 322–333.
50 V. Bernard, V. Mornstein, J. Jaroš, M. Sedláčková and J. Škorpíková, *J. Appl. Biomed.*, 2014, **12**, 137–145.

51 C. Hu, B. Hou and S. Xie, *RSC Adv.*, 2022, **12**, 22722–22747.
52 A. Mysara, M. Morsy, A. O. Ahmed, F. A. Ibrahim and A. Elzwawy, *J. Mater. Sci.*, 2024, **59**, 20964–20981.
53 Y. Yu, J. Geng, E. Y. X. Ong, V. Chellappan and Y. N. Tan, *Adv. Healthcare Mater.*, 2016, **5**, 2528–2535.
54 P. Liang, Q. Guo, T. Zhao, C.-Y. Wen, Z. Tian, Y. Shang, J. Xing, Y. Jiang and J. Zeng, *Anal. Chem.*, 2022, **94**, 8466–8473.
55 X. Meng, S. Sun, C. Gong, J. Yang, Z. Yang, X. Zhang and H. Dong, *ACS Nano*, 2023, **17**, 1174–1186.
56 R. M. Abdelhameed, M. M. Q. Simões, A. M. S. Silva and J. Rocha, *Chem.–Eur. J.*, 2015, **21**, 11072–11081.
57 X. Zhong, X. Wang, L. Cheng, Y. a. Tang, G. Zhan, F. Gong, R. Zhang, J. Hu, Z. Liu and X. Yang, *Adv. Funct. Mater.*, 2020, **30**, 1907954.
58 L.-H. Fu, Y. Wan, C. Qi, J. He, C. Li, C. Yang, H. Xu, J. Lin and P. Huang, *Adv. Mater.*, 2021, **33**, 2006892.
59 T. Sun, R. Wang, W. Lu, X. Shi, F. Gao, T. Wu, G. Wang, X. Su and Z. Teng, *J. Mater. Chem. B*, 2023, **11**, 11280–11289.
60 K. Cheng, X.-Q. Yang, X.-S. Zhang, J. Chen, J. An, Y.-Y. Song, C. Li, Y. Xuan, R.-Y. Zhang, C.-H. Yang, X.-L. Song, Y.-D. Zhao and B. Liu, *Adv. Funct. Mater.*, 2018, **28**, 1803118.
61 G. Yang, L. Xu, J. Xu, R. Zhang, G. Song, Y. Chao, L. Feng, F. Han, Z. Dong, B. Li and Z. Liu, *Nano Lett.*, 2018, **18**, 2475–2484.
62 J. An, Y.-G. Hu, K. Cheng, C. Li, X.-L. Hou, G.-L. Wang, X.-S. Zhang, B. Liu, Y.-D. Zhao and M.-Z. Zhang, *Biomaterials*, 2020, **234**, 119761.
63 Y. Liu, K. Ai and L. Lu, *Chem. Rev.*, 2014, **114**, 5057–5115.
64 X.-C. Liu, G.-C. Wang, R.-P. Liang, L. Shi and J.-D. Qiu, *J. Mater. Chem. A*, 2013, **1**, 3945–3953.
65 Q. Ren, N. Yu, L. Wang, M. Wen, P. Geng, Q. Jiang, M. Li and Z. Chen, *J. Colloid Interface Sci.*, 2022, **614**, 147–159.
66 Z. Dong, L. Feng, Y. Hao, M. Chen, M. Gao, Y. Chao, H. Zhao, W. Zhu, J. Liu, C. Liang, Q. Zhang and Z. Liu, *J. Am. Chem. Soc.*, 2018, **140**, 2165–2178.
67 L. Ding, X. Zhu, Y. Wang, B. Shi, X. Ling, H. Chen, W. Nan, A. Barrett, Z. Guo, W. Tao, J. Wu and X. Shi, *Nano Lett.*, 2017, **17**, 6790–6801.
68 A. León, P. Reuquen, C. Garín, R. Segura, P. Vargas, P. Zapata and P. A. Orihuela, *Appl. Sci.*, 2017, **7**, 49.
69 A. Sosnik, I. Zlotver and H. Potthuri, *Prog. Mater. Sci.*, 2025, **148**, 101384.
70 Y. Harada, K. Ogawa, Y. Irie, H. Endo, L. B. Feril, T. Uemura and K. Tachibana, *J. Contr. Release*, 2011, **149**(2), 190–195.
71 Z. Qin, L. Chen, R. Ma, R. Tomovska, X. Luo, X. Xie, T. Su and H. Ji, *J. Alloys Compd.*, 2020, **836**, 155428.
72 S. Liang, X. Xiao, L. Bai, B. Liu, M. Yuan, P. a. Ma, M. Pang, Z. Cheng and J. Lin, *Adv. Mater.*, 2021, **33**, 2100333.
73 C. Tang, H. Li, M. Sha, J. Song, X. Bai, K. Liu, Y. Liu, B. Yuan, J. Yan, J. Chang and J. Kang, *Chem. Eng. J.*, 2023, **475**, 146054.
74 M. Scrocco, *Chem. Phys. Lett.*, 1979, **61**, 453–456.
75 V. Abdelsayed, S. Moussa, H. M. Hassan, H. S. Aluri, M. M. Collinson and M. S. El-Shall, *J. Phys. Chem. Lett.*, 2010, **1**, 2804–2809.
76 O. Elbanna, M. Fujitsuka, S. Kim and T. Majima, *J. Phys. Chem. C*, 2018, **122**, 15163–15170.
77 Q. Li, Y. Xia, C. Yang, K. Lv, M. Lei and M. Li, *Chem. Eng. J.*, 2018, **349**, 287–296.
78 G. K. Naik, S. M. Majhi, K.-U. Jeong, I.-H. Lee and Y. T. Yu, *J. Alloys Compd.*, 2019, **771**, 505–512.
79 M. Wu, D. Xu, B. Luo, H. Shen, C. Wang and W. Shi, *Mater. Lett.*, 2015, **161**, 45–48.
80 J. Zhang, J. Xi and Z. Ji, *J. Mater. Chem.*, 2012, **22**, 17700–17708.
81 X. Wang, X. Wang, Q. Yue, H. Xu, X. Zhong, L. Sun, G. Li, Y. Gong, N. Yang, Z. Wang, Z. Liu and L. Cheng, *Nano Today*, 2021, **39**, 101170.
82 J. Shao, J. Zhang, C. Jiang, J. Lin and P. Huang, *Chem. Eng. J.*, 2020, **400**, 126009.
83 W. He, K. Ai, C. Jiang, Y. Li, X. Song and L. Lu, *Biomaterials*, 2017, **132**, 37–47.
84 M. Xu, L. Zhou, L. Zheng, Q. Zhou, K. Liu, Y. Mao and S. Song, *Cancer Lett.*, 2021, **497**, 229–242.
85 C. Wang, C. Dai, Z. Hu, H. Li, L. Yu, H. Lin, J. Bai and Y. Chen, *Nanoscale Horiz.*, 2019, **4**, 415–425.
86 B. Hu, A. Huang, X. Zhang, Z. Chen, R. Tu, W. Zhu, Z. Zhuang, C. Chen, Q. Peng and Y. Li, *Nano Res.*, 2021, **14**, 3482–3488.
87 J. Ruan and H. Qian, *Adv. Therapeut.*, 2021, **4**, 2100018.
88 B. Ding, P. Zheng, P. a. Ma and J. Lin, *Adv. Mater.*, 2020, **32**, 1905823.
89 H. Zhang, X. Pan, Q. Wu, J. Guo, C. Wang and H. Liu, *Exploration*, 2021, **1**, 20210010.
90 M. R. Smith, J. Fernandes, Y.-M. Go and D. P. Jones, *Biochem. Biophys. Res. Commun.*, 2017, **482**, 388–398.
91 W. Yue, L. Chen, L. Yu, B. Zhou, H. Yin, W. Ren, C. Liu, L. Guo, Y. Zhang, L. Sun, K. Zhang, H. Xu and Y. Chen, *Nat. Commun.*, 2019, **10**, 2025.
92 G. Zhan, Q. Xu, Z. Zhang, Z. Wei, T. Yong, N. Bie, X. Zhang, X. Li, J. Li, L. Gan and X. Yang, *Nano Today*, 2021, **38**, 101195.
93 Q. Xu, G. Zhan, Z. Zhang, T. Yong, X. Yang and L. Gan, *Theranostics*, 2021, **11**, 1937–1952.
94 H. Sun, J. Su, Q. Meng, Q. Yin, L. Chen, W. Gu, P. Zhang, Z. Zhang, H. Yu, S. Wang and Y. Li, *Adv. Mater.*, 2016, **28**, 9581–9588.
95 R. Yang, J. Xu, L. Xu, X. Sun, Q. Chen, Y. Zhao, R. Peng and Z. Liu, *ACS Nano*, 2018, **12**, 5121–5129.
96 Z. Hu, X. Song, L. Ding, Y. Cai, L. Yu, L. Zhang, Y. Zhou and Y. Chen, *Mater. Today Bio*, 2022, **16**, 100452.
97 S. Bai, N. Yang, X. Wang, F. Gong, Z. Dong, Y. Gong, Z. Liu and L. Cheng, *ACS Nano*, 2020, **14**, 15119–15130.
98 L. Wang, Y. Chen, J. Zhao, D. Luo and W. Tian, *Transl. Cancer Res.*, 2022, **11**, 1970–1976.
99 J. Li, H. Fang, L. Fan, J. Yang, T. Ji and Q. Chen, *Waste Manage.*, 2022, **139**, 96–104.
100 G. Chen, J. Du, L. Gu, Q. Wang, Q. Qi, X. Li, R. Zhang, H. Yang, Y. Miao and Y. Li, *Chem. Eng. J.*, 2024, **482**, 148953.
101 M. Wu, Z. Zhang, Z. Liu, J. Zhang, Y. Zhang, Y. Ding, T. Huang, D. Xiang, Z. Wang, Y. Dai, X. Wan, S. Wang, H. Qian, Q. Sun and L. Li, *Nano Today*, 2021, **37**, 101104.

102 Y. Zhang, Y. Xu, D. Sun, Z. Meng, W. Ying, W. Gao, R. Hou, Y. Zheng, X. Cai, B. Hu and X. Lin, *Chem. Eng. J.*, 2020, **390**, 124521.
103 X. Chen, D. Cheng, M. Ding, N. Yu, J. Liu, J. Li and L. Lin, *J. Mater. Chem. B*, 2022, **10**, 4595–4604.
104 C. He, X. Zhang, C. Chen, X. Liu, Y. Chen, R. Yan, T. Fan, Y. Gai, R. J. Lee, X. Ma, J. Luo, Y. Lu, T. Yang and G. Xiang, *Acta Biomater.*, 2021, **122**, 354–364.
105 R. W. Tarnuzzer, J. Colon, S. Patil and S. Seal, *Nano Lett.*, 2005, **5**, 2573–2577.
106 R. W. Tarnuzzer, J. Colon, S. Patil and S. Seal, *Nano Lett.*, 2005, **5**, 2573–2577.
107 L. Cao, Z. Feng, R. Guo, Q. Tian, W. Wang, X. Rong, M. Zhou, C. Cheng, T. Ma and D. Deng, *Mater. Horiz.*, 2023, **10**, 1342–1353.
108 Y. Qu, Z. Li, W. Chen, Y. Lin, T. Yuan, Z. Yang, C. Zhao, J. Wang, C. Zhao, X. Wang, F. Zhou, Z. Zhuang, Y. Wu and Y. Li, *Nat. Catal.*, 2018, **1**, 781–786.
109 F. Tang, L. Li and D. Chen, *Adv. Mater.*, 2012, **24**, 1504–1534.
110 F. Erogbogbo, K.-T. Yong, R. Hu, W.-C. Law, H. Ding, C.-W. Chang, P. N. Prasad and M. T. Swihart, *ACS Nano*, 2010, **4**, 5131–5138.
111 L. Sun, X. Wang, F. Gong, K. Yin, W. Zhu, N. Yang, S. Bai, F. Liao, M. Shao and L. Cheng, *Theranostics*, 2021, **11**, 9234–9242.
112 R. Que, M. Shao, S. Wang, D. D. Ma and S. T. Lee, *Nano Lett.*, 2011, **11**, 4870–4873.
113 G. Gollavelli and Y.-C. Ling, *Biomaterials*, 2012, **33**, 2532–2545.
114 H. Zhao, J. Duan, Y. Xiao, G. Tang, C. Wu, Y. Zhang, Z. Liu and W. Xue, *Chem. Mater.*, 2018, **30**, 3438–3453.
115 X. Pan, Z. Huang, J. Guo, Q. Wu, C. Wang, H. Zhang, J. Zhang and H. Liu, *Adv. Mater.*, 2024, **36**, 2400142.
116 A. Yildirim, R. Chattaraj, N. T. Blum, G. M. Goldscheitter and A. P. Goodwin, *Adv. Healthcare Mater.*, 2016, **5**, 1290–1298.
117 A. N. Sukumar, P. D. Duraisamy, P. M. S. Paul, P. Gopalan and A. Angamuthu, *J. Biomol. Struct. Dyn.*, 2024, 1–14.
118 Y. Iwase, K. Nishi, J. Fujimori, T. Fukai, N. Yumita, T. Ikeda, F.-S. Chen, Y. Momose and S.-I. Umemura, *Jpn. J. Appl. Phys.*, 2016, **55**, 07KF02.
119 W. Ren, H. Wang, Q. Chang, N. Li, J. Yang and S. Hu, *Carbon*, 2021, **184**, 102–108.
120 S. Yang, X. Wang, P. He, A. Xu, G. Wang, J. Duan, Y. Shi and G. Ding, *Small*, 2021, **17**, 2004867.
121 L. Sun, Y. Cao, Z. Lu, P. Ding, Z. Wang, F. Ma, Z. Wang and R. Pei, *Nano Today*, 2022, **43**, 101434.
122 M. Cheng, Y. Liu, Q. You, Z. Lei, J. Ji, F. Zhang, W.-F. Dong and L. Li, *Adv. Sci.*, 2024, **11**, 2404230.
123 Q. Zhang, J. Liang, S. L. J. Yun, K. Liang, D. Yang and Z. Gu, *Biomater. Sci.*, 2020, **8**, 4129–4146.